Progress in Oceanography 189 (2020) 102446

Contents lists available at ScienceDirect

Progress in Oceanography

journal homepage: www.elsevier.com/locate/pocean

Abyssal food-web model indicates faunal carbon flow recovery and impaired microbial loop 26 years after a sediment disturbance experiment

Daniëlle S.W. de Jonge [a,b,1,2], Tanja Stratmann [b,c,d,*,1], Lidia Lins [e], Ann Vanreusel [e], Autun Purser [f], Yann Marcon [g], Clara F. Rodrigues [h], Ascensão Ravara [h], Patricia Esquete [h], Marina R. Cunha [h], Erik Simon-Lledó [i], Peter van Breugel [b], Andrew K. Sweetman [j], Karline Soetaert [b], Dick van Oevelen [b]

[a] Faculty of Mathematics and Natural Sciences, University of Groningen, P.O. Box 11103, 9700 CC Groningen, the Netherlands
[b] NIOZ Royal Netherlands Institute for Sea Research, Department of Estuarine and Delta Systems, and Utrecht University, P.O. Box 140, 4400 AC Yerseke, the Netherlands
[c] Department of Earth Sciences, Utrecht University, Vening Meineszgebouw A, Princetonlaan 8a, 3584 CB Utrecht, the Netherlands
[d] HGF MPG Joint Research Group for Deep-Sea Ecology and Technology, Max Planck Institute for Marine Microbiology, Celsiusstr. 1, 28359 Bremen, Germany
[e] Marine Biology Research Group, Ghent University, Krijgslaan 281 S8, 9000 Ghent, Belgium
[f] HGF MPG Joint Research Group for Deep-Sea Ecology and Technology, Alfred Wegener Institute, Am Handelshafen 12, 27570 Bremerhaven, Germany
[g] MARUM – Center for Marine Environmental Sciences, General Geology – Marine Geology, University of Bremen, 28359 Bremen, Germany
[h] Departamento de Biologia & Centro de Estudos do Ambiente e do Mar (CESAM), Departamento de Biologia, Universidade de Aveiro, Campus de Santiago, 3810-193 Aveiro, Portugal
[i] National Oceanography Centre, University of Southampton Waterfront Campus, European Way, Southampton SO14 3ZH, UK
[j] Deep-Sea Ecology and Biogeochemistry Research Group, The Lyell Centre for Earth and Marine Science and Technology, Heriot-Watt University, Edinburgh EH14 4AS, UK

ARTICLE INFO

Regional index terms:
South-East Pacific
Peru Basin
DISCOL Experimental Area

Keywords:
Ecosystem disturbance
Deep-seabed mining
Abyssal plains
Ferromanganese nodules
Linear inverse model

ABSTRACT

Due to the predicted future demand for critical metals, abyssal plains covered with polymetallic nodules are currently being prospected for deep-seabed mining. Deep-seabed mining will lead to significant sediment disturbance over large spatial scales and for extended periods of time. The environmental impact of a small-scale sediment disturbance was studied during the 'DISturbance and reCOLonization' (DISCOL) experiment in the Peru Basin in 1989 when 10.8 km^2 of seafloor were ploughed with a plough harrow. Here, we present a detailed description of carbon-based food-web models constructed from various datasets collected in 2015, 26 years after the experiment. Detailed observations of the benthic food web were made at three distinct sites: inside 26-year old plough tracks (IPT, subjected to direct impact from ploughing), outside the plough tracks (OPT, exposed to settling of resuspended sediment), and at reference sites (REF, no impact). The observations were used to develop highly-resolved food-web models for each site that quantified the carbon (C) fluxes between biotic (ranging from prokaryotes to various functional groups in meio-, macro-, and megafauna) and abiotic (e.g. detritus) compartments. The model outputs were used to estimate total system throughput, i.e., the sum of all C flows in the food web (the 'ecological size' of the system), and microbial loop functioning, i.e., the C-cycling through the prokaryotic compartment for each site. Both the estimated total system throughput and the microbial loop cycling were significantly reduced (by 16% and 35%, respectively) inside the plough tracks compared to the other two sites. Site differences in modelled faunal respiration varied among the different faunal compartments. Overall, modelled faunal respiration appeared to have recovered to, or exceeded reference values after 26-years. The model results indicate that food-web functioning, and especially the microbial loop, have not recovered from the disturbance that was inflicted on the abyssal site 26 years ago.

* Corresponding author.
E-mail address: t.stratmann@uu.nl (T. Stratmann).
[1] These authors have contributed equally to this work.
[2] Current address: The Lyell Centre for Earth and Marine Science and Technology, Heriot-Watt University, Edinburgh, Scotland EH12 4AS, UK.

https://doi.org/10.1016/j.pocean.2020.102446
Received 3 April 2020; Received in revised form 21 September 2020; Accepted 22 September 2020
Available online 30 September 2020

1. Introduction

The future demand for metals such as nickel, copper, and cobalt may cause supply shortages from terrestrial mines, thus creating the perceived need to mine these mineral resources elsewhere (Hein et al., 2013). Marine mineral deposits with high metal concentrations, such as polymetallic nodules, polymetallic sulphides, and cobalt-rich ferromanganese crusts, are therefore being prospected, but extraction of these substrates from the seafloor will result in significant environmental impacts. These impacts will include removal of hard substrate, habitat modification and destruction (Oebius et al., 2001), the release of toxic metals (Koschinsky et al., 2003), creation of sediment plumes (Oebius et al., 2001; Murphy et al., 2016), and noise and light pollution (Miller et al., 2018).

To investigate how to achieve the minimum possible effects of mining on deep-sea biota, scientists have performed a variety of experiments, mimicking small-scale disturbances and recording their effects. Previous sediment disturbance experiments to study the response of the deep-sea ecosystem were mainly focused on specific faunal groups (Bluhm, 2001; Ingole et al., 2001, 2005a, 2005b; Miljutin et al., 2011; Rodrigues et al., 2001; Vanreusel et al., 2016). In general, varying degrees of recovery were recorded, with no recovery back to control or baseline conditions for almost all faunal groups over decadal time-scales (Jones et al., 2017). Generally, large sessile species have either not recovered at all or at best, recovered slower than small mobile species (Gollner et al., 2017; Jones et al., 2017) (e.g. large suspension feeders; Simon-Lledó et al., 2019b). Interest in the impact of sediment disturbance on abyssal sediment biogeochemistry has increased relatively recently (Haffert et al., 2020; Paul et al., 2018; Volz et al., 2020).

The most comprehensive of these disturbance studies is the 'DISturbance and reCOLonization' (DISCOL) experiment, which was performed in 1989, during which a manganese nodule area of 10.8 km^2 was ploughed diametrically 78 times with an 8 m-wide plough-harrow, thereby creating plough tracks with nodules mixed into the top 10–20 cm of sediment (Thiel et al., 1989). Next to these plough tracks, the seafloor was not directly disturbed, but the sediment and nodules were covered with a layer of resuspended sediments. Food-web recovery was monitored during five follow-up cruises between March 1989 and September 2015 (Thiel et al., 1989; Schriever, 1990; Schriever and Thiel, 1992; Schriever et al., 1996; Boetius, 2015; Greinert, 2015). In summary, 26 years after the DISCOL experiment the tracks with resettled sediment could still be clearly observed (Gausepohl et al., 2020) (Fig. 1) and the different disturbance levels hosted a distinct megafauna community (Simon-Lledó et al., 2019b). Although deposit-feeder densities, including holothurians, were overall not substantially different among sites after 26 years (Simon-Lledó et al., 2019b; Stratmann et al., 2018c), macrofauna and megafauna densities, especially suspension feeders, were significantly depressed inside the plough track compared to outside the plough tracks and reference sites (Drazen et al., 2019; Simon-Lledó et al., 2019b; Stratmann et al., 2018a). In addition, 26 years after the initial ploughing and mixing of the upper-sediment layer, porewater chemistry in sediments from the DISCOL experimental area (DEA) had recovered, but distinct differences in metal distributions between disturbed and undisturbed sediments still existed (Paul et al., 2018) and microbial mediated biogeochemical functions were still impaired (Vonnahme et al., 2020). Modelling results indicated that removal of the upper sediment layer might result in even slower recovery rates of geochemical sediment processes compared to the recovery process observed when sediments were mixed (Haffert et al., 2020).

So far, the DISCOL follow-up studies focussed on temporal dynamics. However, because not all ecosystem components were addressed during the early years of the experiment, i.e., prokaryotes, meiofauna, and high taxonomic resolution of megafauna were missing, an integrated food-web perspective is lacking in these time-series analyses. During an extensive sampling campaign at the DISCOL site in 2015, data on many ecosystem components, including the smaller metazoan (e.g. nematodes) and microbial domain, were collected. This recent dataset allows the construction of food-web models at spatially separated disturbed and reference sites. Comparing ecosystem functioning at sediments disturbed 26 years ago to sediments at nearby reference sites can help to understand temporal recovery dynamics on decadal time scales.

Food-web models describe the trophic interactions within an ecological community and provide an integrative approach to study ecosystem-wide effects of perturbations, like the DISCOL sediment disturbance (Allesina and Pascual, 2008). The quantification of trophic interactions in a marine network is, however, often hampered by the difficulty of data collection, especially in remote areas like the open or deep ocean. Different methods like top-down mass-balancing (e.g. Hunt et al., 1987) and inverse modelling (Christensen and Pauly, 1992; van Oevelen et al., 2010) have been devised to estimate the fluxes within a food web. Resolved food webs can reveal emergent properties of ecosystem functioning, which can be captured by network indices (Latham, 2006; Heymans et al., 2014).

Network indices can summarize the characteristics of the complex ecological networks at the disturbed and reference sites into single values, which can then be compared among the different disturbance levels. The topological size and complexity can be captured by the number of links (*L*), linkage density (*LD*), i.e., the average number of

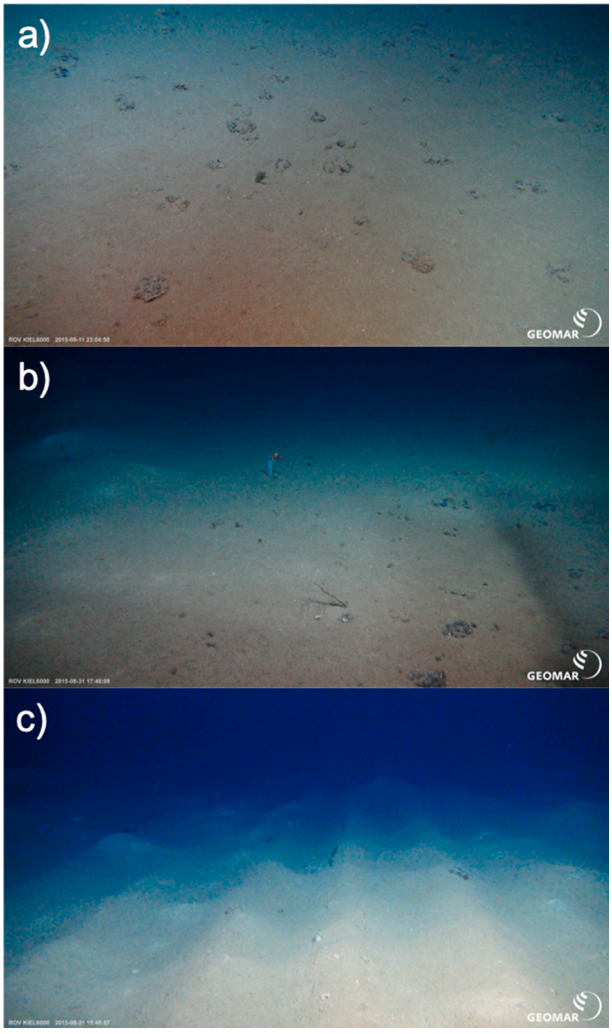

Fig. 1. Representative pictures of the sediments at (a) reference sites, (b) outside plough tracks, and (c) inside plough tracks taken during the Sonne SO242-2 cruise to the DISCOL site in 2015. Photos by ROV Kiel 6000 (GEOMAR, Kiel, Germany).

links per compartments, and connectance (*C*), i.e., the proportion of realised links (Gardner and Ashby, 1970). Trophic level (*TL*) signifies the position of a trophic compartment in the food chain and is related to resource availability and transfer efficiency (Post, 2002). In addition, C cycling is represented by total system throughput (*T..*), i.e. the sum of all C flows in the food web, reflecting the 'ecological' size of the system (Latham, 2006), and by the Finn's Cycling Index (*FCI*), i.e. the proportion of C cycling due to recycling processes, reflecting structural differences and the efficiency of C usage in a system (Finn, 1976). Network indices are robust to a fair extent of variation in input data and network structure (Kones et al., 2009; Heymans et al., 2014). This underlines their suitability for analysing models that cannot be fully parameterized with empirical data, like the food-web model from the remote DISCOL experimental area where direct measurements are limited.

Here, we integrate a recent dataset collected from the DISCOL experiment in 2015 to develop highly resolved food webs of the following sites: inside plough tracks (IPT), outside plough tracks (OPT), i.e., right next to the plough tracks, and reference sites (REF), i.e., an area 4 km from the DEA assumed unaffected by the disturbance. Linear inverse modelling was used to estimate C flows among food-web compartments in pre-defined topological food webs based on information comprising biomass, feeding preferences, growth efficiencies, and respiration rates (Vézina and Platt, 1988; van Oevelen et al., 2010). The resolved linear inverse models for the different disturbance levels allowed us to obtain estimates of C flows that could not be measured *in situ* and determine ecosystem-wide recovery after a small-scale benthic disturbance on decadal timescales. Specifically, system characteristics that we would expect to see at an impacted site are (1) reduced ecosystem complexity due to species mortality reflected by reduced *LD* and *C* indices, (2) reduced mean and maximum TL due to reduced resource availability, impaired metabolic efficiency, and reduction of top predators, (3) reduced productivity of different trophic groups reflected by impaired respiration, and (4) reduced C cycling and recycling efficiency reflected by a reduced *T..* and *FCI* respectively, with a specific focus on C cycling in the microbial loop and the scavenging pathway. Results were compared to other abyssal plain food-web models and

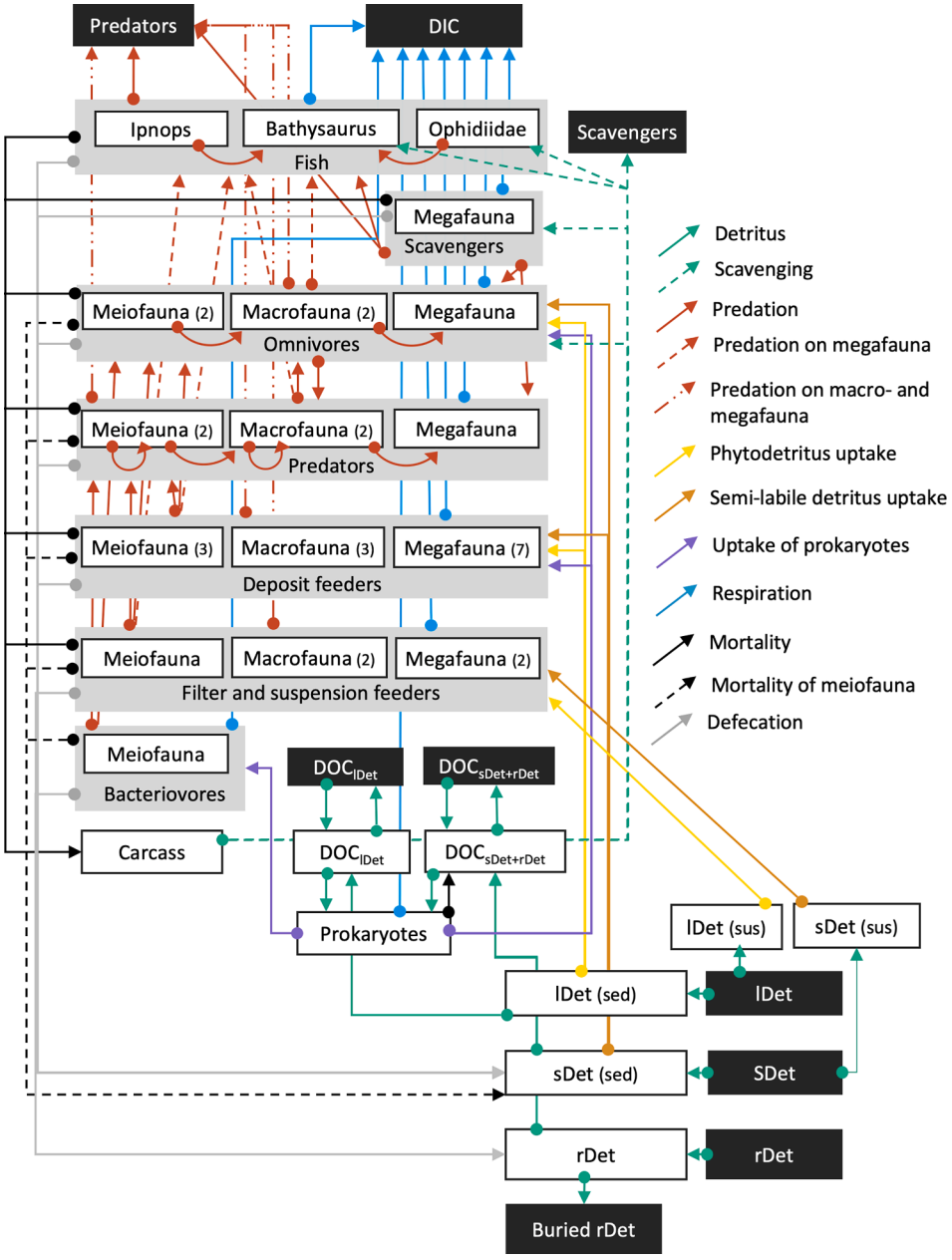

Fig. 2. Schematic representation of the topological food web used for the linear inverse models. White boxes show all food-web compartments inside the model, whereas black boxes show external compartments that were not explicitly modelled. Grey boxes show the feeding types bacterivores, filter and suspension feeders, deposit feeders, predators, omnivores, and fish. The white boxes enclosed by the grey boxes represent the size classes meiofauna, macrofauna, megafauna, and the specific fish taxa *Ipnops* sp., *Bathysaurus mollis*, and Ophidiidae. The numbers in brackets behind the size classes specify the number of food-web compartments of that specific size class and feeding type. The arrows represent C flows leading from the C source (arrow ending with a big dot) to C sink (arrowhead). Abbreviations are: DOC = dissolved organic matter, lDet (sus) = suspended labile detritus, sDet (sus) = suspended semi-labile detritus, lDet (sed) = labile detritus in the sediment, sDet (sed) = semi-labile detritus in the sediments, rDet = refractory detritus.

interpreted with an outlook on deep-seabed mining.

2. Materials & methods

2.1. Study site

The Peru Basin in the south-east Pacific extends from the East Pacific Rise at 110°W to the Atacama Trench west of the coast of Peru (Klein, 1993; Bharatdwaj, 2006). In the North, the Peru Basin borders on the Carnegie Ridge at 5°S and in the South, it borders on the Sala-y-Gomez Ridge and the Nazca Ridge at 24°S (Klein, 1993; Bharatdwaj, 2006). The Peru Basin has a water depth ranging between 3,800 and 4,400 m (Wiedicke and Weber, 1996; Greinert, 2015) and a bottom water temperature of 2.9 °C (Boetius, 2015). The DEA is located in the northern part of the Peru Basin at 07°04.4′S, 88°27.6′W (Thiel et al., 1989). In 2015, the long-term impacts of the original disturbance (1989) were assessed by taking measurements inside plough tracks, outside plough tracks, i.e., areas next to plough-tracks where re-suspended sediment settled, and at reference sites 4 km away from the DEA that were considered to be unaffected by the disturbance (Fig. 1).

2.2. Food-web structure

Faunal compartments in the food web were defined using size-classes (meiofauna MEI, macrofauna MAC, and megafauna MEG) and feeding types (bacterivores B, filter- and suspension feeders FSF, epistrate feeders EF, non-selective deposit-feeders NSDF, sub-surface deposit feeders SSDF, surface deposit feeders SDF, omnivores OF, predators P, scavengers S).

Metazoan meiofauna (>32 μm) consisted of Nematoda, Harpacticoida and their nauplii, Polychaeta, Ostracoda, Tardigrada, Bivalvia, Kinorhyncha, Gastrotricha, Tanaidacea, Cyclopoida, Gastropoda, Loricifera, Oligochaeta, Rotifera, and Isopoda. Based on the four most abundant nematode families in the abyssal CCZ (Miljutin et al., 2011), Nematoda were divided into the feeding types non-selective deposit feeders (NemNSDF), epistrate feeders (NemEF), and omnivores/ predators (NemOP) (Table A1). Meiofauna polychaetes were divided into feeding types following the feeding type classification for macrofauna polychaetes. The remaining metazoan meiofauna were classified as filter and suspension feeders (MeiFSF), bacterivores (MeiB), deposit feeders (MeiDF), predators (MeiP), and omnivore feeders (MeiOF) based on reported feeding ecologies in peer-reviewed literature (Table A1).

Metazoan macrofauna taxa included Polychaeta, Amphipoda, Tanaidacea, Isopoda, Cumacea, Bivalvia, Gastropoda, Scaphopoda, Echinoidea, and Ophiuroidea. The polychaetes were identified to family level, so the review paper by Jumars et al. (2015) was used to classify the polychaetes into suspension feeders (PolSF), surface deposit feeders (PolSDF), subsurface deposit feeders (PolSSDF), predators (PolP), and omnivores (PolOF) (Table A2). For each site, the community composition of polychaete families was used to specify the relative presence of each feeding-type. All other macrofauna taxa were classified as filter and suspension feeders (MacFSF), deposit feeders (MacDF), predators (MacP), and omnivores (MacOF) based on reported feeding ecologies in peer-reviewed literature (Table A2).

Megafauna taxa of the phyla Annelida, Arthropoda, Chordata (except fish), Cnidaria, Echinodermata (except Holothuria), Hemichordata, Mollusca, and Porifera were combined in the feeding types deposit feeders (MegDF), suspension and filter feeders (MegFSF), surface deposit feeders (MegSDF), subsurface deposit feeders (MegSSDF), predators (MegP), omnivores (MegOF), and scavengers (MegS) (Table A3). Furthermore, the five holothurian morphotypes *Amperima* sp., *Benthodytes typica, Mesothuria* sp., *Peniagone* sp. (including *Peniagone* sp. morphotype "palmata", *Peniagone* sp.1, *Peniagone* sp. 2 benthopelagic), and *Psychropotes depressa* that collectively contributed between 80% (OPT) and 83% (REF) to the total holothurian biomass (Stratmann et al., 2018c) were kept as separate food-web compartments (Table A3). All other holothurian morphotypes were summed as filter and suspension feeding holothurians (HolFSF) and surface-deposit feeding holothurians (HolSDF) based on their feeding ecology (Table A3).

Fish were divided into *Bathysaurus mollis*, *Ipnops* sp., and Ophidiidae. *Bathysaurus mollis* predates on *Ipnops* sp., Ophidiidae, Amphipoda, Cirripedia, Isopoda, Munidopsidae, *Probeebei* sp., Pycnogonida, and other crustaceans, and it also scavenges carrion (Sulak et al., 1985; Crabtree et al., 1991; Drazen and Sutton, 2017). *Ipnops* sp. predates upon Polychaeta, Amphipoda, Isopoda, other crustaceans, and Mollusca (Crabtree et al., 1991; Drazen and Sutton, 2017). Ophidiidae predates on Polychaeta, Amphipoda, Isopoda, other crustaceans, Mollusca and it scavenges carrion (Crabtree et al., 1991; Drazen and Sutton, 2017; Gerringer et al., 2017). The contribution of the different megafaunal compartments to the fish diet (Table A4) was calculated based on the contribution of each prey taxon to the feeding-type specific C stock.

The non-faunal food-web compartments included prokaryotes (Pro), carrion (CARC), dissolved organic carbon (DOC), and detritus divided into different lability classes, namely labile detritus (lDet), semi-labile detritus (sDet), and refractory detritus (rDet) (*sensu* van Oevelen et al., 2012).

2.3. Food-web links

Carbon transfer links in the food web were implemented as shown in Fig. 2. Suspended and sedimentary (semi-)labile detritus and sedimentary refractory detritus receive C input from an external (semi-)labile detritus and an external refractory detritus pool. Suspended labile and semi-labile detritus were C sources for all filter- and suspension feeders (MeiFSF, MacFSF, PolSF, MegFSF, and HolFF). Nematode epistrate feeders (NemEF) fed on sedimentary labile detritus and prokaryotes. Sedimentary labile detritus, semi-labile detritus, and prokaryotes were grazed upon by non-selective deposit feeders (NemNSDF), surface deposit feeders (PolSDF and HolSDF), subsurface deposit feeders (PolSSDF), other deposit feeders (MeiDF, MacDF, and MegDF), deposit-feeding holothurians (*Amperima* sp., *Benthodytes* sp., *Mesothuria* sp., *Peniagone* sp., and *Psychropotes* sp.), and omnivores (NemOP, MeiOF, PolOF, MacOF, and MegOF).

Predators and omnivores predated on all faunal organisms from the same and smaller size classes. Meiofauna and macrofauna predators (NemOP, MeiP, PolP, MacP) also predated on their own compartment. Additionally, omnivores and scavengers (MegS, *Bathysaurus mollis*, and Ophidiidae) scavenged from the carrion compartment. *Ipnops* sp. predated upon MegFSF, MegDF, MegP, and MegS (Table A4). *Bathysaurus mollis* predated upon MegFSF, MegDF, MegP, MegS, *Ipnops* sp., and Ophidiidae, and Ophidiidae predated upon MegFSF, MegDF, MegP, and MegS (Table A4).

All faunal compartments produced faeces that contributed to the semi-labile and refractory detritus pool. Furthermore, nematode and other metazoan meiofauna mortality contributed to the semi-labile detritus pool, whereas dead polychaetes, other metazoan macrofauna, holothurians, other megafauna, and fishes contributed to the carrion pool. Sedimentary labile, semi-labile, and refractory detritus hydrolysed to DOC, which was taken up by prokaryotes.

Prokaryotes respired C as dissolved inorganic carbon (DIC) and contributed to the DOC pool by virus-induced prokaryotic lysis. The DOC pool further increased by influx of external DOC to the system. Other C fluxes out of the model included the burial of refractory detritus, respiration by all faunal compartments, the efflux of DOC, external scavengers scavenging carrion, and predation on polychaetes, other macrofauna, holothurians, other megafauna, and fishes by external predators.

For the incorporation of isotope data, several processes (detritus uptake, defecation, and respiration) were specifically divided into labile detritus-derived fluxes and semi-labile and/or refractory detritus-derived fluxes (see 'Incorporation of isotope tracer data').

2.4. Data sources

2.4.1. Carbon stocks of food-web compartments

To quantify the labile, semi-labile, and refractory detritus, and prokaryote pools in the upper 5 cm of sediment of the different study sites, sediment samples were taken with multi corers from inside the chambers of benthic landers after lander retrieval, and ROV-deployed push corers and blade corers (Table A5).

The labile detritus pool is defined as the average chlorophyll-a (chl-a) content in the surface sediment (*sensu* van Oevelen et al., 2011a), and was measured by Vonnahme et al. (2020, IPT corresponded to the microhabitats 'Furrow' and 'Ridge' combined). Chl-a was extracted in 90% acetone, measured photometrically following Jeffrey's and Humphrey (1975) approach for mixed phytoplankton populations and converted to C units using a C to chl-a-ratio of 40 (De Jonge, 1980).

The semi-labile detritus pool is defined as the sum of proteins, carbohydrates, and lipids, i.e., the so-called biopolymeric carbon (Fabiano et al., 1995). The concentration of total hydrolysable amino acids (THAA) in 0.4 g freeze-dried surface sediment per sample was measured following Maier et al. (2019). As neither lipid nor carbohydrate concentrations in the sediment were measured, a ratio of 0.12 : 1 : 1.32 for lipids : THAAs : carbohydrates (Laubier and Monniot, 1985) was used to calculate the total biopolymeric carbon pool.

The refractory detritus pool refers to the particulate organic carbon (POC) stock in the surface sediment that was measured by Vonnahme et al. (2020, IPT corresponded to the microhabitats 'Furrow' and 'Ridge' combined) and from which the labile and semi-labile detritus pools were subtracted.

Prokaryotic abundance in the surface sediment (0–1 cm) was determined by Vonnahme et al. (2020, IPT corresponded to the microhabitats 'Furrow' and 'Ridge' combined) using the Acridine Orange Direct Count (AODC) method. Subsequently, we converted prokaryotic abundances into prokaryotic C stock (mmol C m^{-2}) by multiplying the abundance with a factor of 12.5 fg C $cell^{-1}$, i.e., C content of prokaryotic cells in waters from the southern subtropical Pacific (15°S) (Fukuda et al., 1998). The 0–1 cm prokaryotic C stock was extrapolated to the 0–5 cm prokaryotic C stock as:

$$Cstock_{0-5cm} = \sum Cstock_{0-1cm} \times e^{-0.1\times(x+1)} \quad (1)$$

based on previous C stock measurements in the Peru Basin (Forschungsverbund Tiefsee-Umweltschutz, unpubl.). $Cstock_{0-1cm}$ corresponds to the C stock in the surface sediment (0–1 cm) and $(x + 1)$ is the sediment interval (i.e., $x = 1$ for the sediment interval 1–2 cm).

Metazoan meiofaunal C stock was determined from ROV-deployed push corers (7.4 cm inner-diameter) (Table A5) of which the upper 5 cm of sediment was preserved in 4% borax-buffered formaldehyde at room temperature. Ashore, sediment samples were washed over a 32-µm sieve and metazoan meiofauna was extracted by density centrifugation with Ludox HS40 (Dupont) at 3000 rpm. A subset of 100–150 metazoan meiofauna specimens per sample were identified to higher taxonomic level, i.e. to the rank of order, subclass, class, or phyla using Higgins and Thiel (1988), and counted with a stereomicroscope (Leica MZ8, 50× magnification) to determine taxon-specific densities. When the number of metazoan meiofauna individuals was lower than 100, the whole sample was counted. Stocks of all metazoan meiofauna taxa were calculated by multiplying the taxon-specific densities with the conversion factors from Table A1. Stocks of the different taxa were grouped according to feeding type as described above (see 'Food-web structure').

Metazoan macrofauna were collected with a 50 × 50 × 60 cm box-corer at all three sites (Table A5). The sediment of the upper 5 cm was sieved on a 500-µm sieve and all organisms that were retained on this sieve were preserved in 96% un-denaturated ethanol and stored at −20 °C. Ashore, all macrofauna samples were sorted under stereomicroscopes (Olympus SZX9, Olympus SZH10, Leica MZ125) and a compound microscope (Olympus BX50 MO). They were identified to higher taxon level, i.e., to the rank of order, subclass, class, or phyla. Macrofauna polychaetes were identified to family level. For the identifications a vast list of papers was used specialized in the different taxa at major group level as well as at family, genus, and even species level. Macrofauna and macrofaunal polychaete stocks were calculated by multiplying the macrofauna and macrofaunal polychaete densities from the box corers with taxon-specific individual biomass data from Table A2.

Table 1
Carbon stocks (mmol C m^{-2}) of the food-web compartments at reference sites (REF), outside plough tracks (OPT), and inside plough tracks (IPT).

Compartment	REF	OPT	IPT
Detritus			
Labile detritus (lDet)	6.37	5.70	5.25
Semi-labile detritus (sDet)	406	538	367
Refractory detritus (rDet)	6955	7168	7808
Prokaryotes			
Prokaryotes (Pro)	8.52	8.48	8.17
Meiofaunal Nematoda			
Non-selective deposit feeding nematodes (NemNSDF)	0.22	0.42	0.33
Epistrate feeding nematodes (NemEF)	0.11	0.21	0.17
Omnivory/ predatory nematodes (NemOP)	0.11	0.21	0.17
Metazoan meiofauna (except Nematoda)			
Meiofauna filter and suspension feeders (MeiFSF)	3.87×10^{-2}	6.70×10^{-2}	4.34×10^{-2}
Meiofauna bacterivores (MeiBF)	4.66×10^{-4}	8.09×10^{-4}	1.07×10^{-3}
Meiofauna deposit feeders (MeiDF)	1.33	2.09	1.82
Meiofauna predators (MeiP)	6.61×10^{-2}	6.85×10^{-2}	3.51×10^{-2}
Meiofauna omnivores (MeiO)	0.18	0.37	0.48
Macrofaunal Polychaeta			
Polychaete suspension feeders (PolSF)	0.14	0.21	0.24
Polychaete surface deposit feeders (PolSDF)	0.40	0.46	0.52
Polychaete subsurface deposit feeders (PolSSDF)	0.17	0.16	0.20
Polychaete predators (PolP)	0.24	0.22	0.21
Polychaete omnivores (PolO)	0.11	0.18	0.07
Macrofauna (except Polychaeta)			
Macrofauna filter feeders (MacFSF)	3.61×10^{-2}	3.87×10^{-2}	2.63×10^{-2}
Macrofauna deposit feeders (MacDF)	1.35	0.38	0.11
Macrofauna predators (MacP)	0.18	8.48×10^{-2}	5.09×10^{-2}
Macrofauna omnivore (MacO)	4.05×10^{-2}	4.24×10^{-2}	5.04×10^{-2}
Holothuroidea			
Amperima sp.	6.01×10^{-2}	7.17×10^{-2}	5.85×10^{-2}
Benthodytes typica	6.76×10^{-2}	0.10	0.12
Mesothuria sp.	1.84×10^{-2}	1.27×10^{-2}	1.26×10^{-2}
Peniagone sp.	2.12×10^{-2}	1.68×10^{-2}	1.89×10^{-2}
Psychropotes depressa	5.11×10^{-2}	7.97×10^{-3}	1.43×10^{-2}
Filter and suspension feeding holothurians (HolFSF)	0.00	0.00	4.56×10^{-3}
Surface-deposit feeding holothurians (HolSDF)	4.35×10^{-2}	5.23×10^{-2}	4.41×10^{-2}
Megafauna (except Holothuroidea)			
Megafauna filter and suspension feeders (MegFSF)	9.22	7.44	4.15
Megafauna deposit feeders (MegDF)	2.51	2.33	3.49
Megafauna predators (MegP)	3.35	2.50	5.91
Megafauna scavengers (MegS)	1.43×10^{-2}	1.51×10^{-2}	6.19×10^{-2}
Megafauna omnivores (MegO)	0.93	1.22	2.22
Fishes			
Bathysaurus sp.	0.00	4.73	14.7
Ipnops sp.	0.21	0.23	0.12
Ophidiidae	0.00	0.11	1.00

Table 2
Data on carbon fluxes (mmol C m^{-2} d^{-1}) that were fed into the model as inequalities [minimum, maximum] or equalities (single values). Abbreviations are: REF = reference sites, OPT = outside plough tracks, IPT = inside plough tracks. References: [1]Haeckel et al. (2001), [2]Ståhl et al. (2004), [3]Buchanan (1984), [4]Lahajnar et al. (2005), [5]Paul et al. (2018), [6]This study, [7]Vonnahme et al. (2020), [8]Danovaro (2010).

Carbon flux	Value	References
Labile + semi-labile detritus deposition	[0.18, 0.33]	1
Refractory detritus deposition	[4.11 × 10^{-3}, ∞[a]]	1
Labile + semi-labile detritus degradation rate	[2.19 × 10^{-5}, ∞[a]] × C stock	1
Refractory detritus degradation rate	[2.74 × 10^{-9}, ∞[a]] × C stock	1
Burial flux of refractory detritus	REF: 8.95 × 10^{-2} OPT: 8.95 × 10^{-2} IPT: 9.92 × 10^{-2}	1, 2, 3, 6
Diffusive flux of DOC from the sediment	−2.69 × 10^{-3} OPT: 7.37 × 10^{-5} IPT: −8.71 × 10^{-5}	4, 5, 6
Total C mineralization[b]	REF (n = 25): [0.69, 0.90] OPT (n = 28): [0.53, 0.70] IPT (n = 19): [0.51, 0.68]	7
Prokaryotic C production[b]	REF (n = 6): [0.34, 0.68] OPT (n = 8): [0.40, 1.00] IPT (n = 14): [0.11, 0.37]	7, 8

[a] The original upper bounds from Haeckel et al. (2001) for refractory detritus deposition and degradation rates resulted in incompatible constraints in the LIM, therefore the upper bounds were removed.
[b] Minimum and maximum values correspond to the 1st and 3rd quartile of the dataset.

Subsequently, the different C stocks were combined in feeding types as described above (see 'Food-web structure').

Densities and subsequently biomass of holothurians at all three sites were measured on >4500 seafloor photographs taken with the towed "Ocean Floor Observation System" (OFOS LAUNCHER) (Drazen et al., 2019) as described by Stratmann et al. (2018c). C stocks of the holothurian morphotypes were calculated as the product of the morphotype-specific densities (Stratmann et al., 2018c) and the median morphotype specific individual biomasses (Table A3) and grouped into individual holothurian food-web compartments as described under 'Food-web structure'.

Density of other metazoan megafauna taxa (ind m^{-2}) was determined on seafloor images taken with the towed OFOS LAUNCHER as described in Drazen et al. (2019). For each disturbance level (REF, OPT, IPT), 300 pictures were randomly selected and annotated with the open-source annotation software PAPARA(ZZ)I (Marcon and Purser, 2017). Densities of all metazoan megafauna were converted to C stocks (mmol C m^{-2}) by appropriate conversion factors (Table A3).

Fishes seen on OFOS pictures were identified to family and when possible to genus level using the "Atlas of Abyssal Megafauna Morphotypes of the Clipperton-Clarion Fracture Zone: Osteichthyes" identification guide (Linley, 2014). Subsequently, fish densities were converted to C stocks (mmol C m^{-2}) using fish-taxon dependent conversion factors (Table A4). The stock of each food-web compartment as used in the linear inverse model is summarized in Table 1.

2.4.2. Site-specific flux constraints

Data constraints on the C fluxes in the food web are presented in Table 2. Labile + semi-labile detritus deposition refers to the sum of labile and semi-labile detritus deposition to the system, whereas refractory detritus deposition is the deposition of refractory detritus to the system. Correspondingly, labile + semi-labile degradation rate relates to the total loss of labile and semi-labile detritus via dissolution of detritus to DOC and uptake by fauna. Refractory detritus degradation is the dissolution of refractory detritus to DOC. These four fluxes were

Table 3
Physiological processes prokaryotic growth efficiency *PGE* (–), virus-induced prokaryotic mortality *VIPM* (–), assimilation efficiency *AE* (–), net growth efficiency *NGE* (–), secondary production *SP* (mmol C m^{-2} d^{-1}), mortality *M* (mmol C m^{-2} d^{-1}), respiration *R* (mmol C m^{-2} d^{-1}), feeding selectivity *FS* (–), and feeding preference *FP* (–) implemented in the food-web models for different size classes or compartments either as equality (single values) and inequality constraints ([minimum, maximum] values). References: [1]Vonnahme et al. (2020), [2]Danovaro et al. (2008), [3]Herman and Vranken (1988), [4]Grahame (1973), [5]Johnson (1976), [6]Jordana et al. (2001), [7]Niu et al. (1998), [8]Peña-Messina et al. (2009), [9]Sejr et al. (2004), [10]Arifin and Bendell-Young (1997), [11]Bayne et al. (1993), [12]Cammen et al. (1980), [13]Connor et al. (2016), [14]Cox and Murray (2006), [15]Enríquez-Ocaña et al. (2012), [16]Griffiths (1980), [17]Han et al. (2008), [18]Hughes (1971), [19]Ibarrola et al. (2000), [20]Kreeger and Newell (2001), [21]Labarta et al. (1997), [22]Lee (1997), [23]Mondal (2006), [24]Navarro et al. (1992), [25]Navarro and Thompson (1996), [26]Nelson et al. (2012), [27]Nieves-Soto et al. (2013), [28]Nordhaus and Wolff (2007), [29]Camacho et al. (2000), [30]Petersen et al. (1995), [31]Ren et al. (2006), [32]Resgalla et al. (2007), [33]Savari et al. (1991), [34]Smaal and Vonck (1997), [35]Tatián et al. (2008), [36]Velasco and Navarro (2003), [37]Wright and Hartnoll (1981), [38]Yu et al. (2013), [39]Zhou et al. (2006), [40]Drazen et al. (2007), [41]Clausen and Riisgård (1996), [42]Navarro et al. (1994), [43]Nielsen et al. (1995), [44]Koopmans, Martens and Wijffels (2010), [45]Childress et al. (1980), [46]Ceccherelli and Mistri (1991), [47]Fleeger and Palmer (1982), [48]Mistri et al. (2001), [49]Vranken and Heip (1986), [50]Brey et al. (1998), [51]Brey and Hain (1992), [52]Cartes and Sorbe (1999), [53]Soliman and Rowe (2008), [54]Baumgarten et al. (2014), [55]Brey et al. (1995), [56]Brey and Clarke (1993), [57]Cartes et al. (2011), [58]Cartes et al. (2001), [59]Gorny et al. (1993), [60]Collins et al. (2005), [61]Randall (2002), [62]Shirayama (1992), [63]Sommer et al. (2010), [64]van Oevelen et al. (2009), [65]Brown et al. (2018), [66]Hughes (2010), [67]Hughes et al. (2011), [68]Khripounoff et al. (2017), [69]Nunnally et al. (2016), [70]Treude et al. (2002), [71]Witte and Graf (1996), [72]Drazen and Seibel (2007), [73]Drazen and Yeh (2012), [74]Smith (1978), [75]Smith and Brown (1983), [76]Smith and Hessler (1974), [77]Smith and Laver, (1981), [78]this study, [79]Miller et al. (2000), [80]van Oevelen et al. (2012), [81]Purinton et al. (2008).

Process	Size class/compartment	Value	References
PGE	Prokaryotes	REF: [0.27, 0.50] OPT: [0.36, 0.65] IPT: [0.14, 0.42]	1
VIPM	Prokaryotes	[0.87, 0.91]	2
AE	Metazoan meiofauna[a,c]	[0.18, 0.27]	3
	Macrofauna[a]	[0.68, 0.89]	4–9
	Megafauna[a]	[0.40 0.75]	8, 10–39
	Fish	[0.84, 0.87]	40
NGE	Metazoan meiofauna[e]	[0.10, 0.96]	–
	Macrofauna	[0.57, 0.68]	41–43
	Megafauna	[0.23, 0.61]	23, 43, 44
	Fish	[0.37, 0.71]	45
SP	Metazoan meiofauna[a]	[2.00 × 10^{-2}, 0.12] × C stock	46–49
	Macrofauna[b]	[2.57 × 10^{-3}, 1.67 × 10^{-2}] × C stock	50 –53
	Megafauna[b]	[3.18 × 10^{-4}, 1.47 × 10^{-3} [d]] × C stock	54–59
	Fish	[0, 6.30 × 10^{-4}] × C stock	60, 61
M	Metazoan meiofauna	[0, 0.12] × C stock	–
	Macrofauna	[0, 1.67 × 10^{-2}] × C stock	–
	Megafauna	[0, 1.47 × 10^{-3}] × C stock	–
	Fish	[0, 6.30 × 10^{-4}] × C stock	–
R	Metazoan meiofauna[b,c]	[7.00 × 10^{-3}, 0.15] × C stock	62
	Macrofauna	[3.57 × 10^{-5}, 4.21 × 10^{-2}] × C stock	62–64
	Megafauna[c]	[9.32 × 10^{-8}, 1.26 × 10^{-3}] × C stock	65–71
	Ophidiidae	5.91 × 10^{-4}	72

(continued on next page)

Table 3 (*continued*)

Process	Size class/compartment	Value	References
	Bathysaurus sp., *Ipnops* sp.	[1.79×10^{-4}, 8.54×10^{-4}] × C stock	72–77
FS	NemNSDF, MeiDF, MacDF, MegDF, PolSSDF, *Mesothuria* sp.[d]	[1, 15]	78–80
	PolSDF, HolSDF, *Amperima* sp. *Benthodytes typica*, *Peniagone* sp. *Psychropotes depressa*	[50, 1000]	80, 81
FP	NemOP	[0.75, 1.0]	80

[a] Due to a lack of data for abyssal plains, the data from near-shore areas were applied.

[b] Due to a lack of data for abyssal plains, the data from the continental slope were applied.

[c] The range of constraints was extended as explained in the methods section in order to avoid incompatible constraints in the LIM.

[d] The minimum constraint was set to zero for *Mesothuria* sp., in order to avoid incompatible constraints in the LIM.

[e] *NGE* for meiofauna was calculated as described in Eq. (7) ($NGE = \frac{SP}{(SP+R)}$) using *SP* and *R* from meiofauna in this table.

estimated by Haeckel et al. (2001) in a numerical diagenetic model for the Peru Basin based on organic matter and pore water profiles of oxygen, nitrate, nitrite, ammonia, phosphate, manganese, sulphate, silicate, and pH.

Burial of refractory detritus (*BFc*) was calculated following Ståhl et al. (2004) as:

$$BF_c = \omega \times DBD \times sedOC \quad (2)$$

where ω is the sediment accumulation rate (2 cm ky^{-1}; Haeckel et al., 2001), *DBD* is the dry bulk density (2.65 g cm^{-3}; Buchanan, 1984), and *sedOC* is the sediment organic C content of the 14–16 cm sediment layer (REF: $0.74 \pm 5.45 \times 10^{-2}$ wt%, $n = 6$; OPT: $0.74 \pm 4.77 \times 10^{-2}$ wt%, $n = 9$; IPT: $0.82 \pm 5.43 \times 10^{-2}$ wt%, $n = 18$).

The diffusive DOC flux out of the sediment (J_0) was inferred from the DOC concentration difference in the overlaying water and the pore water in the surface sediment (0–2 cm). It was calculated with Fick's First Law:

$$J_0 = -\varphi^m \times D_{sw} \times \frac{dC}{dz_0} \quad (3)$$

where φ^m is the porosity of the surface sediment, D_{sw} is the molecular diffusion coefficient of DOC, dC is the DOC concentration gradient between porewater and bottom water, and dz_0 is the distance over which the concentration gradient was measured (Lahajnar et al., 2005). Porosity of surface sediment was measured (REF: 0.93 ± 0.01, OPT: 0.93 ± 0.01, IPT: 0.92 ± 0.01) by weight loss due to freeze-drying (Haffert et al., 2020, IPT corresponded to the microhabitats 'Furrow' and 'Ridge' combined). The difference in DOC concentration between porewater at the midpoint of the sampling interval, i.e., 1 cm for a 0–2 cm sediment slice, and bottom water was 11.32 µmol DOC L^{-1} (REF), −0.31 ± 0.95 µmol DOC L^{-1} (OPT), and 0.37 ± 0.71 µmol DOC L^{-1} (IPT) (Paul et al., 2018). The molecular diffusion coefficient of DOC for deep-sea regions is 2.96×10^{-7} cm^2 s^{-1} (Lahajnar et al., 2005).

Total C respiration was measured as diffusive oxygen uptake (DOU) rates by ROV deployed *in situ* microsensors (MPI, Bremen) and by microprofiling with a benthic flux lander system (MPI, Bremen) (Vonnahme et al., 2020, IPT corresponded to the microhabitats 'Furrow' and 'Ridge' combined).

Prokaryotic C production was measured as ^{3}H-leucin incorporation by prokaryotes (Vonnahme et al., 2020, IPT corresponded to the microhabitats 'Furrow' and 'Ridge' combined) and converted to prokaryotic production following Danovaro (2010):

$$PCP = LI \times (\%Leu) \times M \times 0.86, \quad (4)$$

where *PCP* is the prokaryotic C production (in mmol C m^{-2} d^{-1}). *LI* is the leucine incorporation rate (nmol Leu g dry sediment^{-1} d^{-1}), %*Leu* is the leucine fraction in the total prokaryotic amino acid pool (0.073), *M* is the molar weight of leucine (131.2 g mol^{-1}) and 0.86 is the conversion factor of prokaryotic protein production to prokaryotic C production.

2.4.3. Physiological constraints

Physiological constraints used in the model are presented in Table 3. Prokaryotic growth efficiency (*PGE*) at REF, OPT, and IPT were estimated based on measured PCP and on prokaryotic respiration measured as DOU (Vonnahme et al., 2020; IPT corresponded to the microhabitats "Furrow" and "Ridge" combined) as:

$$PGE = \frac{PCP}{(PCP + DOU)} \quad (5)$$

The minimum and maximum values of virus-induced prokaryotic mortality (*VIPM*) corresponded to the $mean_{VIPM} - SD_{VIPM}$ and the $mean_{VIPM} + SD_{VIPM}$ values for sediments below 1000 m water depth (Danovaro et al., 2008).

Assimilation efficiency *AE* was defined as:

$$AE = \frac{(I - F)}{I} \quad (6)$$

with *I* being the ingested food and *F* being the faeces (Crisp, 1971). Net growth efficiency *NGE* was defined as:

$$NGE = \frac{G}{(G + R)} \quad (7)$$

where *G* was the growth and *R* was the respiration (Clausen and Riisgård, 1996). To determine the minimum and maximum conversion constraints of *AE* and *NGE* in the model, a water depth-dependent dataset of published *AE* and *NGE* values for invertebrate metazoan meiofauna, macrofauna, and megafauna was compiled (see literature references in Table 3). Subsequently, descriptive statistics were applied to the datasets and the lower quartile was used as minimum constraint and the upper quartile as maximum constraint. However, due to constraint incompatibility found during model development, the minimum *AE* constraint for metazoan meiofauna was changed from lower quartile to the minimum value. Net growth efficiency for metazoan meiofauna was calculated with Eq. (7) using the minimum and maximum secondary production rates *SP* (for *G*) and respiration rates in Table 3. The minimum and maximum *AE* values for fish were set to the range of *AE* measured for shallow and deep-water fishes (Drazen et al., 2007).

The minimum and maximum invertebrate secondary production rates *SP* (mmol C m^{-2} d^{-1}) were calculated as:

$$SP = \frac{P}{B} ratio \times C \ \ stock \quad (8)$$

where $\frac{P}{B}$-*ratio* was the lower and upper quartile production/biomass-ratio (d^{-1}) for invertebrate meiofauna, macrofauna, and megafauna from the descriptive statistical analysis of a depth-dependent dataset of published $\frac{P}{B}$-*ratio* values (see literature references in Table 3) as described for *AE* and *NGE*. The maximum secondary production *SP* (mmol C m^{-2} d^{-1}) for fish was also calculated with Eq. (8), but with a $\frac{P}{B}$-*ratio* based on the allometric relationship between annual $\frac{P}{B}$-*ratio* (yr^{-1}) and fish weight *W* (g) (Randall, 2002):

$$\log_{10} \frac{P}{B} ratio = 0.42 - 0.35 \times 5.86 \times \log_{10}(W) \quad (9)$$

The fish weight *W* (g) used in Eq. (9) was the individual biomass of a benthic deep-sea fish as calculated for a water *depth* of 4100 m as (Collins et al., 2005):

$$\log_{10} W = 0.62 + 5.86 \times 10^{-41} \times depth \quad (10)$$

Table 4
Phytodetritus C incorporation rates I (mmol phytodetritus C mmol C^{-1} d^{-1}) in prokaryotes, several Nematoda feeding types, macrofauna, and holothurians based on pulse-chase experiments by Stratmann et al. (2018b). The data are presented as inequalities [minimum, maximum] or equalities (single values). See Table 1 for full compartment names, sites are abbreviated as: REF = reference sites, OPT = outside plough tracks, IPT = inside plough tracks.

Size class	Food-web compartments	Phytodetritus C incorporation	
Prokaryotes		REF + OPT:	$[4.62 \times 10^{-3}, 1.46 \times 10^{-2}]$
		IPT:	$[2.49 \times 10^{-3}, 1.02 \times 10^{-2}]$
Nematoda	NemNSDF, NemEF	REF + OPT:	$[1.53 \times 10^{-3}, 2.95 \times 10^{-3}]$
		IPT:	$[1.23 \times 10^{-3}, 3.23 \times 10^{-3}]$
Polychaeta	PolSDF		$[3.79 \times 10^{-3}, 4.62 \times 10^{-3}]$
Macrofauna	MacDF		$[9.40 \times 10^{-5}, 1.20 \times 10^{-3}]$
	MacFSF		$[2.49 \times 10^{-4}, 1.25 \times 10^{-3}]$
Holothurians	*Amperima* sp.		$[1.24 \times 10^{-3}, 1.13 \times 10^{-2}]$
	Benthodytes typica, Mesothuria sp., *Peniagone* sp., *Psychropotes depressa*, HolSDF		$[1.24 \times 10^{-3}, 1.29 \times 10^{-2}]$

The mortality M (mmol C m^{-2} d^{-1}) always ranged from 0 to the maximum secondary production SP.

Similar to SP, the respiration R (mmol C m^{-2} d^{-1}) was calculated as:

$$R = r \times Cstock \tag{11}$$

where r was the lower and upper quartile biomass-specific faunal respiration (d^{-1}) for invertebrate meiofauna, macrofauna, and megafauna from the descriptive statistical analysis of a depth-dependent dataset of published biomass-specific faunal respiration rates (see literature references in Table 3). Due to otherwise incompatible constraints, the respiration constraints for metazoan meiofauna were set to the minimum and maximum biomass-specific faunal respiration presented in Table 3. R of fish was calculated as described in Eq. (11): Ophidiidae r was based on a measurement for Ophidiidae (Drazen and Seibel, 2007) and r of the food-web compartments *Bathysaurus* sp. and *Ipnops* sp. was based on a dataset of 7 demersal fish species (*Antimora microlepis*, *Pachycara gymninium*, *Sebastolobus altivelis*, *Coryphaenoides acrolepis*, *Cyclothone acclinidens*, *Corphaenoides armatus*, *Synaphobranchus kaupi*; $n = 26$; (Smith and Hessler, 1974; Smith, 1978; Smith and Laver, 1981; Smith and Brown, 1983; Drazen and Seibel, 2007; Drazen and Yeh, 2012).

Feeding selectivity FS described the proportionally higher uptake of labile detritus to semi-labile detritus compared to their presence in the detritus stock (van Oevelen et al., 2012). Feeding preference FP of mixed omnivores and predators signified the contribution of predation to their diet.

2.4.4. Incorporation of isotope tracer data

Stratmann et al. (2018b) investigated site-specific differences (REF vs. IPT) in the incorporation of fresh phytodetritus C by prokaryotes, metazoan meiofauna, macrofauna, and holothurians (Table 4) by conducting *in situ* pulse-chase experiments with ^{13}C-labelled *Skeletonema costatum*. These phytodetritus C incorporation rates I were integrated in the linear inverse model to further constrain C flows (van Oevelen et al., 2006, 2012). The secondary production based on phytodetritus C incorporation SP_P was implemented as:

$$SP_P = I \times B \tag{12}$$

and as:

$$SP_P = U_P \times AE \times NGE \tag{13}$$

where U_P is the uptake of phytodetritus C (mmol C m^{-2} d^{-1}).

2.5. Linear inverse model development

Carbon-based linear inverse models were developed for steady state conditions, with sink compartments and fluxes between these food-web compartments (see 'Food-web structure' and 'Food-web links'). The food-web model is a set of linear functions formed by an equality and inequality matrix equation (van Oevelen et al., 2010):

$$\boldsymbol{E} \cdot \boldsymbol{x} = \boldsymbol{f} \tag{14}$$

$$\boldsymbol{G} \cdot \boldsymbol{x} \geq \boldsymbol{h} \tag{15}$$

where vector $\boldsymbol{x}$ contains the unknown fluxes, vectors $\boldsymbol{f}$ and $\boldsymbol{h}$ contain empirical equality and inequality data respectively (see 'Data availability'), whereas the coefficients in matrices $\boldsymbol{E}$ and $\boldsymbol{G}$ specify the combination of unknown fluxes that should meet the requirements defined in vectors $\boldsymbol{f}$ and $\boldsymbol{h}$.

When all compartments are present in the food web, it contained 430 C flows with 41 mass-balances, i.e. food-web compartments, 6 data equalities, and 453 data inequalities. This implies that the model was mathematically under-determined (47 equalities vs. 430 unknown flows). The models were solved in the R package *LIM* v.1.4.6 (van Oevelen et al., 2010) in R 3.6 (R-Core Team, 2017) on the bioinformatics server of the Royal Netherlands Institute of Sea Research (The Netherlands). Following the likelihood approach (van Oevelen et al., 2010), 100,000 model solutions were generated in 25 parallel sessions, i.e., 4000 solutions per session. For each flow, means and standard deviations of the 100,000 solutions were calculated, which showed a convergence of standard deviations to ±2% error margin. The model input and R-code are included as supplementary material.

2.6. Network indices

Network indices number of links (L), linkage density (LD), connectance (C) Total system throughput ($T..$), i.e., the sum of all C flows in the food web, Finns' Cycling Index (FCI), and the trophic level (TL) of each faunal compartment were calculated with the R package *NetIndices* v.1.4.4. (Kones et al., 2009) for each of the 100,000 model solutions and summarized as mean ± SD. The trophic level of the carrion pool $TL_{carrion}$ was calculated for each model solution as the weighted average of inflow source compartments as:

$$TL_{carrion} = \sum_{j=1}^{n} \left(T^*_{j,carrion} / T_{carrion} \times TL_j \right) \tag{16}$$

where n is the number of internal food-web compartments, j are food-web compartments, T^* is the flow matrix excluding external flows, and $T_{carrion}$ is the total inflow to the carrion compartment excluding external sources.

2.7. Statistical analysis

Statistical differences between disturbance levels for individual C flows, C flow pathways and network indices were determined using the approach presented in van Oevelen et al. (2011b). Briefly, the fraction of flows in one randomized set that is larger than flows in another randomized set in a pairwise comparison is calculated and used to define significance. When the similarity between sites is <10%, i.e. <10% or >90% of the flows in one set are larger, the difference is considered to be significant. When the similarity between sites is <5%, i.e. <5% or >95% of the flows in one set are larger, the difference is considered highly significant.

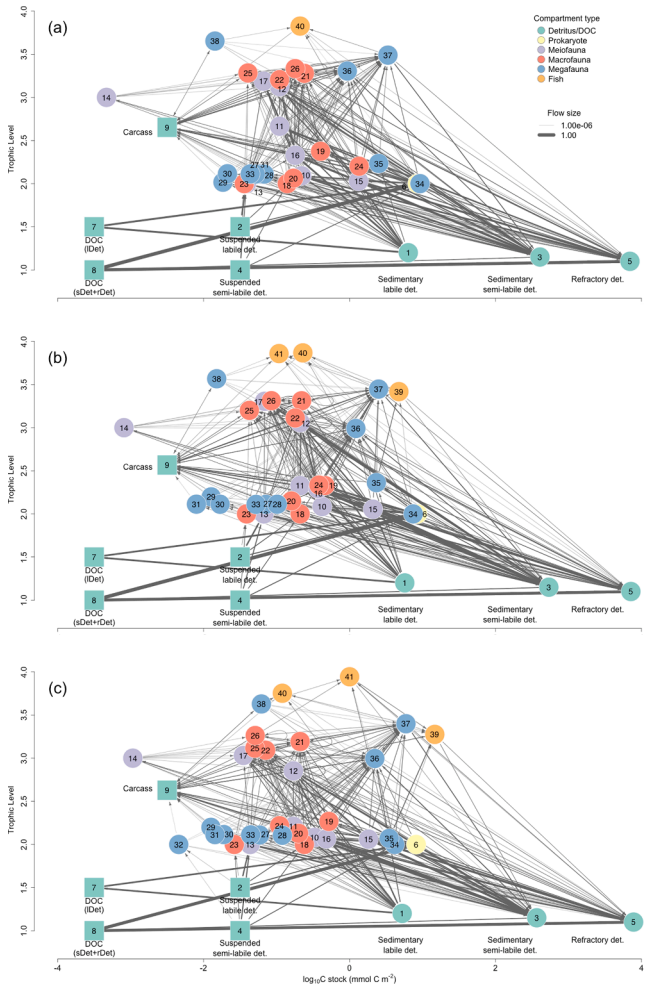

Fig. 3. Food-web model structure of the (a) reference sites, (b) outside plough tracks, and (c) inside plough tracks. Square nodes represent compartments for which carbon stock values were assigned for plotting purposes. Also, the trophic level of the square nodes (except for the carcass compartment) was altered from its true value of 1.0 for plotting purposes. The thickness of a link denotes the flow magnitude transformed by a double square-root (mmol C m^{-2} d^{-1}). Note that import and export from the system have not been plotted. Numbers inside every node correspond to the compartments as follows: 1 = sedimentary labile detritus, 2 = suspended labile detritus, 3 = sedimentary semi-labile detritus, 4 = suspended semi-labile detritus, 5 = sedimentary refractory detritus, 6 = prokaryotes, 7 = labile detritus-based DOC in the sediment, 8 = semi-labile and refractory detritus-based DOC in the sediment, 9 = carrion, 10 = non-selective deposit feeding nematodes, 11 = epistrate feeding nematodes, 12 = omnivory predatory nematodes, 13 = metazoan meiofauna filter and suspension feeder, 14 = metazoan meiofauna bacterivore, 15 = metazoan meiofauna deposit feeder, 16 = metazoan meiofauna predator, 17 = metazoan meiofauna omnivore, 18 = polychaete suspension feeder, 19 = polychaete surface deposit feeder, 20 = polychaete subsurface deposit feeder, 21 = polychaete predator, 22 = polychaete omnivore, 23 = macrofauna filter feeder, 24 = macrofauna deposit feeder, 25 = macrofauna omnivore, 26 = macrofauna predator, 27 = *Amperima* sp., 28 = *Benthodytes typica*, 29 = *Mesothuria* sp., 30 = *Peniagone* sp., 31 = *Psychropotes depressa*, 32 = filter and suspension feeding holothurians, 33 = surface-deposit feeding holothurians, 34 = megafauna filter and suspension feeder, 35 = megafauna deposit feeder, 36 = megafauna omnivore, 37 = megafauna predator, 38 = megafauna scavengers, 39 = *Bathysaurus mollis*, 40 = *Ipnops* sp., and 41 = Ophidiidae.

2.8. Additional incorporation of xenophyophores and dark C fixation

Protozoa and dark C fixation (DCF) are known to occur in abyssal systems (Gooday et al., 1992; Molari et al., 2013; Sweetman et al., 2019), but were omitted from the main food-web model due to a severe lack of data. To aid the discussion of this important model limitation, the limited available site-specific data on these two food-web components were additionally incorporated into the three models to observe the effects on the overall food-web solutions. Detailed methods for this additional incorporation are given in the Appendix and Table A6. In summary, site-specific xenophyophore densities from image annotations were combined with the average xenophyophore test size in the Clarion-Clipperton Fracture Zone (CCZ) (Simon-Lledó et al., 2019a), and regression and conversion data from literature to obtain an estimated biomass assuming all observed specimens were alive. Xenophyophore trophic relations and physiological rates were incorporated based on both general benthic foraminifera and specific xenophyophore literature. DCF rates were calculated from the site-specific rates reported by Vonnahme et al. 2020 using the upper 1 cm and sediment dry bulk density and porosity values given in 'Site-specific flux constraints'. It was assumed that the uptake of DIC by prokaryotes leads to effective prokaryotic biomass production and that all DOC production from DIC comes from prokaryotic viral lysis. It is crucial to bear in mind that these additional processes are poorly constrained, and any quantitative interpretation of results must be done with great caution.

Table 5
Network indices calculated for the food webs at reference sites (REF), outside plough tracks (OPT), and inside plough tracks (IPT). *n* = Number of food-web compartments, *L* = Total number of links, *LD* = Linkage density, *C* = connectance.

Site	*n*	*L*	*LD*	*C*
REF	38	360	9.47	0.213
OPT	40	382	9.55	0.203
IPT	41	391	9.54	0.198

Table 6
Comparison of different network measures calculated for reference sites (REF), outside plough tracks (OPT), and inside plough tracks (IPT). The numbers indicate the fraction of values of the first site that are higher than the values of the second site in a random pairwise comparison. * Significant difference, ** highly significant difference.

Network measure	REF vs. OPT	REF vs. IPT	OPT vs. IPT
Trophic level			
Mean	0.21	0.68	0.89
Carrion	0.67	0.55	0.36
Carnivores	0.42	0.49	0.57
Deposit feeders	0.46	0.50	0.55
Respiration			
Total	1.00**	1.00**	0.64
Prokaryotes	1.00**	1.00**	0.54
Meiofaunal nematodes	0.07*	0.01**	0.09*
Metazoan meiofauna (except nematodes)	0.06*	0.22	0.84
Macrofaunal polychaetes	0.13	0.38	0.76
Macrofauna (except polychaetes)	0.63	1.00**	1.00**
Holothurians	1.00**	1.00**	0.34
Megafauna (except holothurians)	0.07*	0.02**	0.38
Fish	0.00**	0.00**	0.00**
Faunal (all excl. prokaryotes)	0.02**	0.02**	0.70
Faunal (macro- and megafauna)	0.08*	0.08*	0.54
Carbon cycling			
Total carbon throughput *T*..	0.22	1.00**	1.00**
Finn's cycling index *FCI*	0.00**	0.15	1.00**
Specific carbon pathways			
Microbial loop	0.71	1.00**	1.00**
Scavenging pathway	0.22	0.58	0.86
Prokaryotic DOC uptake	0.06*	1.00**	1.00**
Ingestion of prokaryotic C	0.01**	1.00**	1.00**

Table 7
Detritus deposition (mmol C m^{-2} d^{-1}) of different lability classes and food-web respiration (mmol C m^{-2} d^{-1}) of the different size classes at reference sites (REF), outside plough tracks (OPT), and inside plough tracks (IPT). Data are presented as mean ± SD and contribution (in %) of size class-specific respiration to total respiration.

	REF	%	OPT	%	IPT	%
Total deposition	0.88 ± 3.19 × 10^{-2}	100	0.71 ± 4.87 × 10^{-2}	100	0.71 ± 3.72 × 10^{-2}	100
Labile detritus	0.29 ± 1.84 × 10^{-2}	33.1	0.28 ± 3.22 × 10^{-2}	38.8	0.25 ± 2.20 × 10^{-2}	35.8
Semi-labile detritus	3.70 × 10^{-2} ± 1.77 × 10^{-2}	4.20	4.98 × 10^{-2} ± 2.63 × 10^{-2}	7.02	7.32 × 10^{-2} ± 2.26 × 10^{-2}	10.3
Refractory detritus	0.55 ± 1.91 × 10^{-2}	62.4	0.38 ± 2.53 × 10^{-2}	54.1	0.38 ± 1.98 × 10^{-2}	53.8
DOC influx	2.69 × 10^{-3} ± 1.09 × 10^{-3}	0.31	0.00[a]		8.71 × 10^{-5} ± 3.56 × 10^{-5}	0.01
Total respiration	0.78 ± 2.15 × 10^{-2}	100	0.62 ± 3.08 × 10^{-2}	100	0.61 ± 2.07 × 10^{-2}	100
Prokaryotes	0.73 ± 1.94 × 10^{-2}	92.4	0.53 ± 2.57 × 10^{-2}	85.7	0.53 ± 1.81 × 10^{-2}	86.7
Metazoan meiofauna (except Nematodes)	3.37 × 10^{-2} ± 9.07 × 10^{-3}	4.27	5.36 × 10^{-2} ± 1.67 × 10^{-2}	8.71	3.95 × 10^{-2} ± 9.55 × 10^{-3}	6.52
Nematoda	5.12 × 10^{-3} ± 1.44 × 10^{-3}	0.65	8.12 × 10^{-3} ± 2.10 × 10^{-3}	1.32	1.51 × 10^{-2} ± 6.08 × 10^{-3}	2.49
Macrofaunal polychaetes	9.37 × 10^{-3} ± 1.11 × 10^{-3}	1.19	1.10 × 10^{-2} ± 1.58 × 10^{-3}	1.78	9.80 × 10^{-3} ± 1.63 × 10^{-3}	1.62
Macrofauna (except polychaetes)	4.89 × 10^{-3} ± 9.32 × 10^{-4}	0.62	4.42 × 10^{-3} ± 7.00 × 10^{-4}	0.72	2.04 × 10^{-3} ± 2.46 × 10^{-4}	0.34
Holothurians	3.56 × 10^{-4} ± 5.23 × 10^{-5}	0.05	2.91 × 10^{-4} ± 6.13 × 10^{-5}	0.05	3.01 × 10^{-4} ± 6.29 × 10^{-5}	0.05
Megafauna (except holothurians)	6.29 × 10^{-3} ± 1.06 × 10^{-3}	0.80	9.78 × 10^{-3} ± 1.85 × 10^{-3}	1.59	1.05 × 10^{-2} ± 1.41 × 10^{-3}	1.73
Fish	9.24 × 10^{-5} ± 3.19 × 10^{-5}	0.01	1.06 × 10^{-3} ± 6.96 × 10^{-5}	0.17	3.32 × 10^{-3} ± 3.25 × 10^{-5}	0.55
Faunal (all excl. prokaryotes)	5.98 × 10^{-2} ± 9.36 × 10^{-3}	7.59	8.82 × 10^{-2} ± 1.71 × 10^{-2}	14.3	8.05 × 10^{-2} ± 1.15 × 10^{-2}	13.3

[a] No DOC influx was measured, hence modelled, outside the plough tracks.

3. Results

3.1. Food-web structure and trophic levels

The food-web models at REF, OPT, and IPT contained 38, 40, and 41 compartments, respectively (Fig. 3, Table 5). No filter-feeding holothurians were observed at the OPT and REF sites, so these compartments were omitted from those models. In addition, the fish taxa *Bathysaurus mollis* and Ophidiidae were not observed at the REF sites and therefore these compartments were not included in the REF food-web model. Food-web model compartments were connected with 360 (REF) to 391 (IPT) links, with a linkage density between 9.47 (REF) and 9.55 (OPT) and a connectance of 0.198 (IPT) to 0.231 (REF) (Table 5).

Maximum trophic levels at the three sites were estimated as 3.83 ± 0.21 (REF), 3.87 ± 0.22 (OPT), and 3.94 ± 0.08 (IPT). The mean modelled trophic level ranged from 2.57 ± 0.57 (IPT) to 2.65 ± 0.82 (OPT) and did not differ significantly between sites (Table 6). Mean modelled trophic levels of carnivores were estimated at 3.27 ± 0.39 (REF), 3.29 ± 0.43 (OPT), and 3.20 ± 0.46 (IPT), whereas mean modelled trophic levels of deposit feeders were estimated at 2.23 ± 0.29 (REF), 2.24 ± 0.27 (OPT), and 2.20 ± 0.25 (IPT). For both feeding types (carnivores and deposit feeders), the difference between sites was not significant (Table 6).

3.2. Carbon flows

Modelled total C input (mmol C m^{-2} d^{-1}) (Table 7), i.e., deposition and filter/suspension feeding, was estimated to be 0.88 ± 3.19 × 10^{-2} (REF), 0.71 ± 4.87 × 10^{-2} (OPT), and 0.71 ± 3.72 × 10^{-2} (IPT). Modelled total C input was dominated by refractory detritus deposition that contributed between 53.8% (IPT) and 62.4% (REF) to total C input. The contribution of labile detritus deposition and filter/suspension feeding on this detritus type to modelled total C input was between 33.1% (REF) and 38.8% (OPT) and semi-labile detritus accounted for 4.2% (REF) to 10.3% (IPT). DOC influx (mmol C m^{-2} d^{-1}) was estimated to be 2.69 × 10^{-3} ± 1.09 × 10^{-3} (0.3% of total C input) at REF and 8.71 × 10^{-5} ± 3.56 × 10^{-5} (0.01% of total C input) IPT.

The models estimated most C was lost via respiration (85.9% at IPT to 88.6% at REF), followed by C burial whose contribution was 10.2% (REF), 12.6% (OPT), and 14.0% (IPT). DOC efflux resulted in an estimated loss of 7.37 × 10^{-5} ± 3.00 × 10^{-5} mmol C m^{-2} d^{-1} at OPT (1.04 × 10^{-2}% of total C outflow); no DOC efflux was measured (and therefore modelled) at REF and IPT (Table 2).

Estimated respiration (mmol C m^{-2} d^{-1}) ranged from 0.61 ± 2.07 × 10^{-2} (IPT) to 0.79 ± 2.15 × 10^{-2} (REF) and was significantly higher at REF compared to OPT and IPT (Table 6). Estimated respiration was dominated by modelled prokaryotic respiration that contributed between 85.7% (OPT) and 92.4% (REF) to total respiration. Faunal, i.e., non-prokaryotic respiration, was estimated to be significantly lower at REF (5.98 × 10^{-2} ± 9.36 × 10^{-3} mmol C m^{-2} d^{-1}) compared to OPT (8.82 × 10^{-2} ± 1.71 × 10^{-2} mmol C m^{-2} d^{-1}) and IPT (8.05 × 10^{-2} ± 1.15 × 10^{-2} mmol C m^{-2} d^{-1}) (Table 6).

Estimated C ingestion is summarized in Fig. 4. Estimated uptake of C by metazoan meiofauna was largest (REF: 0.67 ± 4.73 × 10^{-2} – OPT: 0.88 ± 8.73 × 10^{-2} mmol C m^{-2} d^{-1}) of which 3.0–5.2% by filter and suspension feeders, 35.8–56.4% by all deposit feeders, 34.4–56.6% by all omnivores, and 2.8–6.2% by all predators. Estimated C uptake by macrofauna (IPT: 4.11 × 10^{-2} ± 4.49 × 10^{-3} – OPT: 5.34 × 10^{-2} ± 6.54 × 10^{-3} mmol C m^{-2} d^{-1}) and megafauna (REF: 2.94 × 10^{-2} ± 3.98 × 10^{-3} – IPT: 5.43 × 10^{-2} ± 7.02 × 10^{-3} mmol C m^{-2} d^{-1}) were of similar magnitude. Estimated macrofauna C uptake was done for 11.2–17.5% by all filter and suspension feeders, for 48.5–53.0% by all deposit feeders, for 11.3–16.2% by all omnivores, and for 18.3–28.9% by all predators. Estimated megafauna C uptake was mediated for 23.9–33.4% by all filter and suspension feeders, for 16.4–24.4% by all deposit feeders, for 18.8–32.7% by all omnivores, and for 19.0–31.7% by all predators. Fig. 4 indicates a reduced ingestion of prokaryotic C, and increased importance of feeding on detritus for deposit feeders and omnivores IPT compared to REF and OPT, which is confirmed by a significance test (Table 6).

Uptake of DOC by prokaryotes, which is part of the microbial loop (see 'Specific carbon pathways'), was 1.75 ± 7.11 × 10^{-2} mmol C m^{-2} d^{-1} at REF, 2.00 ± 1.03 × 10^{-1} mmol C m^{-2} d^{-1} at OPT, and 1.07 ± 5.66 × 10^{-2} mmol C m^{-2} d^{-1} at IPT. DOC uptake by prokaryotes significantly decreased from REF to OPT and from OPT to IPT (Table 6).

A summary of the most important changes in modelled C flows among the three sites is visualized in Fig. 5. Highlights in the diagram

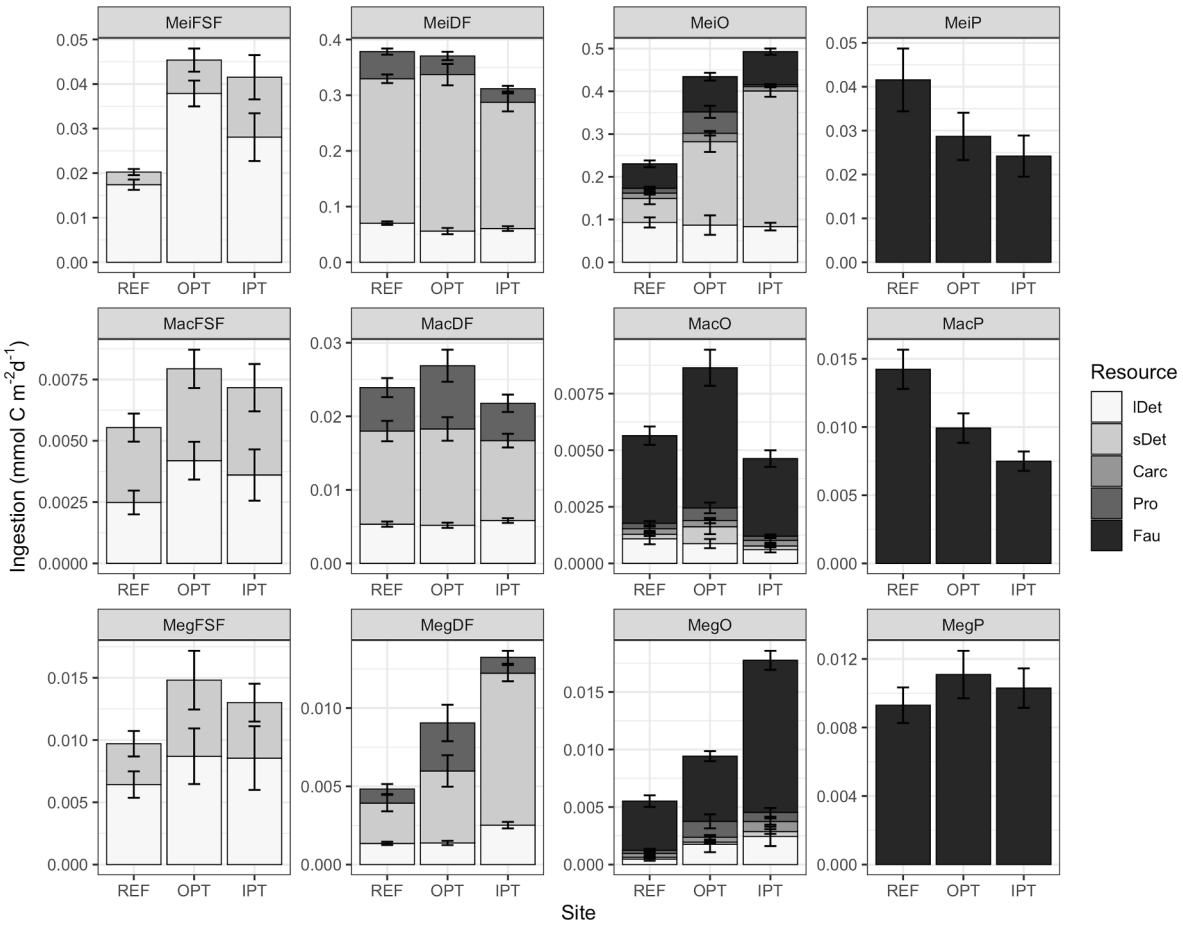

Fig. 4. Estimated uptake of carbon (mmol C m^{-2} d^{-1}) through ingestion of labile detritus (lDet), semi-labile detritus (sDet), carrion (Carc), prokaryotes (Pro), or fauna (Fau) for different consumer groups. For plotting purposes, the y-scale varies per panel, and some consumer groups include multiple food-web compartments: MeiDF = NemNSDF + NemEF + MeiDF + MeiB, MeiO = NemOP + MeiO, MacFSF = PolSF + MacFSF, MacDF = PolSDF + PolSSDF + MacDF, MacO = PolO + MacO, MacP = PolP + MacP, MegFSF = HolFF + MegFSF, MegDF = Amp + Benth + Meso + Penia + Psych + HolSDF + MegDF, MegO = MegO + MegS + Bathy + Ophid, MegP = MegP + Ipnop. Error bars represent one standard deviation.

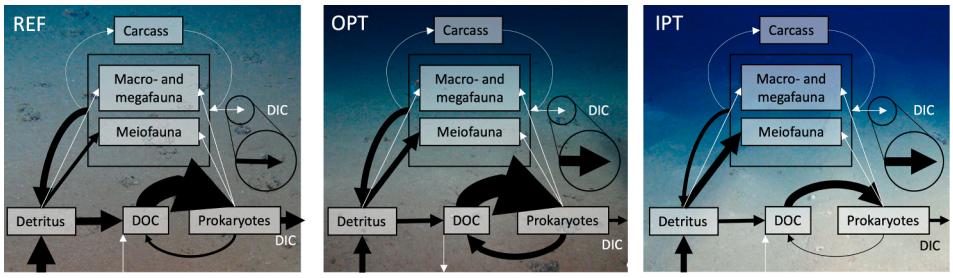

Fig. 5. Diagram summarizing the most important changes in modelled carbon flows among the reference site (REF), outside the plough tracks (OPT), and inside the plough tracks (IPT). The width of the black arrows corresponds to the flow magnitude (mmol C m^{-2} d^{-1}) squared. The white arrows have flow magnitudes too small to scale in the figure. The enlarged white flows are enlarged 100x for comparison with the scaled (i.e. black) arrows. The background images are equal to Fig. 1.

include the differences in detritus deposition and dissolution. The microbial loop, including DOC uptake and prokaryotic respiration, is significantly reduced at IPT (Table 6), and metazoan meiofaunal ingestion dominates overall faunal ingestion whereas ingestion of macro- and megafauna combined is much smaller. Faunal respiration is significantly smaller at the REF (Table 6). The scavenging loop is relatively small and not significantly different among sites (Table 6), whereas input to the detritus compartment through excretion by, and mortality of metazoan meiofauna is large.

Additional incorporation of poorly constrained xenophyophores and DCF results in similar total C inflow, overall respiration, faunal respiration, and observed differences between sites (Table A7). Also, the uptake rate of xenophyophores is estimated to have the same order of magnitude as the uptake rate of metazoan meiofauna in the main model (Table A7).

3.3. C cycling

Total C throughput *T*.. (mmol C m^{-2} d^{-1}) was estimated to be 5.61 ± 0.11 (REF), 5.77 ± 0.19 (OPT), and 4.74 ± 0.14 (IPT). The modelled *T*.. at IPT was significantly smaller compared to the other two sites, but the difference in modelled *T*.. between REF and OPT was not significant

(Table 6). Finn's cycling index *FCI* was estimated as $0.24 \pm 1.65 \times 10^{-2}$ (REF), $0.35 \pm 2.00 \times 10^{-2}$ (OPT), and $0.26 \pm 1.08 \times 10^{-2}$ (IPT), and was significantly higher at OPT (Table 6). The difference in estimated *FCI* between REF and IPT was not significant. Additional incorporation of poorly constrained xenophyophores and DCF results in increased *T*.. (by approximately 10–15%) and *FCI* (by approximately 10–50%) values, however, with the same trend in differences between sites as the main model (Table A7).

3.4. Specific carbon pathways

The microbial loop, i.e., detritus dissolution, DOC uptake by prokaryotes, viral-induced prokaryotic lysis, prokaryotic respiration, and faunal grazing on prokaryotes, had an estimated C flow of $3.34 \pm 7.70 \times 10^{-2}$ mmol C m^{-2} d^{-1} at REF, which was 59.5% of modelled *T*… The microbial loop accounted for an estimated 3.25 ± 0.11 mmol C m^{-2} d^{-1} (56.3% of modelled *T*..) at OPT. The estimated microbial loop IPT of $2.2 \pm 6.32 \times 10^{-2}$ mmol C m^{-2} d^{-1} (46.2% of modelled *T*..) was significantly smaller compared to the other two sites (Table 6).

The models estimated that only 65.9% of C that passed through the microbial loop at REF flowed through the microbial loop IPT. Similar values for microbial loop C cycling were found when additionally incorporating poorly constrained xenophyophores and DCF (Table A7).

An estimated C flow of $1.36 \times 10^{-2} \pm 6.96 \times 10^{-3}$ mmol C m^{-2} d^{-1} was channelled through the scavenging pathway, i.e., carrion scavenging, at REF, which was 0.24% of modelled *T*… The C flow through the scavenging pathway was estimated to be $2.13 \times 10^{-2} \pm 1.07 \times 10^{-2}$ mmol C m^{-2} d^{-1} at OPT (0.37% of modelled *T*..), and estimated to be $1.17 \times 10^{-2} \pm 3.52 \times 10^{-3}$ mmol C m^{-2} d^{-1} at IPT (0.25% of modelled *T*..). The modelled amount of C that was channelled through the scavenging pathway did not differ significantly among sites (Table 6).

A summary of the modelled microbial loop and scavenging loop is included in Fig. 5.

4. Discussion

The degree of ecosystem recovery of an abyssal plain food web from the DISCOL sediment disturbance experiment was assessed by investigating differences in modelled C flows between reference sites, outside plough tracks, and inside plough tracks that were created 26 years prior to sampling. The benthic abyssal food web, estimated by linear inverse modelling, was relatively complex with a link density (i.e. realisation of all possible links in a food web) of ~20% (Smith-Ramesh et al., 2017). On average, each food-web model compartment had roughly 10 interactions with other compartments (Table 5), and the modelled mean and maximum trophic level were 2.6 and 3.8, respectively. The food web was estimated to be mainly fuelled by deposition of refractory detritus, whereas modelled export was mainly via respiration and deep burial (Table 7), the latter simply being refractory C export independent of infauna activity and bioturbation rates. Modelled microbial respiration accounted for roughly 90% of overall estimated respiration, whereas modelled metazoan meiofaunal (incl. nematodes) respiration was always more than half of the estimated total faunal respiration (Table 7). Modelled metazoan meiofaunal (incl. nematodes) C ingestion was roughly an order of magnitude larger than the combined modelled C ingestion by macrofauna and megafauna (Fig. 4). After 26 years, the modelled microbial loop within the plough tracks was still impaired (Table 6), so that the total modelled C flows inside plough tracks had not recovered to reference values. In contrast, estimated faunal respiration appeared to have recovered and sometimes exceeded the modelled values found at the reference sites, although this varied among food-web compartments.

4.1. Model limitations

Though the model was based on an extensive dataset generated using state-of-the-art technologies and methods, it unavoidably comes with limitations.

The sampling of faunal groups was focused on determining diversity and density estimates. As such, the faunal biomass values were derived using conversion factors which, especially for metazoan meiofauna, are not well constrained. Physiological data and feeding preferences were taken from literature, and although care was taken to use data calculated from large datasets including representative species, the constraints might deviate from the biological traits of the modelled functional groups.

Fish were observed in relatively low densities (34 ind. ha^{-1}) compared to smaller fauna, but they have high body masses thereby contributing considerably to the biomass of the system. Although the sample size in this study was relatively small (0.4 ha), our estimated density is similar to the average fish density in the DISCOL area of 30 ind. ha^{-1} reported by Drazen et al. (2019) and 18 to 63 ind. ha^{-1} reported by Simon-Lledó et al. (2019a) over an area of approximately 10 ha. This larger area studied by Drazen et al. (2019) showed that also Liparidae, Macrouridae and Zoarcidae fish were reported in the DISCOL area in addition to *Bathysaurus mollis*, *Ipnops* sp. and Ophidiidae used in our food web model. However, their sightings by Drazen et al (2019) were rare (4, 7, and 4 individuals of Liparidae, Macrouridae and Zoarcidae respectively over ~10 ha), explaining their absence in our imagery analysis. Similarly, the densities of *Bathysaurus mollis* and Ophidiidae found by Drazen et al. (2019) were very low: 2 and 19 sightings respectively at the reference site, compared to 5 and 30 sightings respectively outside the plough tracks, and 2 and 10 sightings respectively inside the plough track. For comparison, Ipnopidae sightings ranged between 13 and 100 times. These low densities of *Bathysaurus mollis* and Ophidiidae found by Drazen et al. (2019) explains their absence at the reference sites in our model. A more extensive analysis of fish presence and biomass might improve the model; we expect that such inclusion will mostly affect network indices related to network topology, like maximum trophic level, with only minor changes in overall faunal C cycling as currently fish respiration only contributes 0.1% to 4.1% of modelled faunal respiration.

Prominent model limitations are the lack of distinction between Bacteria and Archaea, the exclusion of the dark inorganic C fixation (DCF) process, and missing protozoan food-web compartments. These model limitations stem from a severe lack of data, and future research into these components is highly recommended. The modelled prokaryotic food-web compartment includes both Bacteria and Archaea as there were not enough data available to include them as separate compartments. The relative contribution of Archaea to total prokaryotic biomass at the DISCOL site is unknown, but might be limited (<10%, Hoshino and Inagaki, 2019). Additionally, the extent of archivory, i.e. metazoan grazing on Archaea, is very poorly known (Thurber et al., 2012).

Both abyssal Bacteria and Archaea are thought to be able to perform DCF either as autotrophic process, as anaplerotic reaction in the heterotrophic process, or a combination of both in a mixotrophic process (Middelburg, 2011; Molari et al., 2013; Sweetman et al., 2019; Vonnahme et al., 2020; Woulds et al., 2020). The estimated DCF fluxes, ranging from roughly 0.2 mg C m^{-2} d^{-1} (~1200 m in the Mediterranean, Molari et al. 2013) to 2 mg C m^{-2} d^{-1} (~4150 m in the Peru Basin, Vonnahme et al. 2020) are very large and comparable to estimated POC flux to the seafloor in the Peru Basin (2.16–3.96 mg C m^{-2} d^{-1}, Haeckel et al. 2001). However, as the exact DCF pathway in Bacteria and/or Archaea is still largely unknown it was not yet possible to confidently include this process in our main DISCOL food-web model.

The benthic abyssal protozoa community, i.e. single-celled

eukaryotes including protists, has a size range from nano- (Gooday et al., 1995) to megabenthic scale (Rodrigues et al., 2001), and is very poorly characterized. Although test-forming protists called foraminifera often dominate faunal densities in deep-sea benthic systems, data on biomass contribution and metabolism is extremely limited (Gooday et al., 2020 and references therein). There is practically no data on the abundance and importance of deep sedimentary naked protists (e.g. flagellates, ciliates, and amoebas) (Gooday et al., 2020) and other protozoa like fungi. Despite the severe lack of data, protists are thought to play an important role in C cycling as they can directly consume bacteria (Laureillard et al., 2004; Mojtahid et al., 2011), other protists, detritus (Levin and Gooday, 1992), and perhaps even small metazoans (Levin, 1991) and DOM (DeLaca et al., 1981; Nomaki et al., 2011). Protists are preyed upon by some metazoans and other protists, and some protist species might provide a habitat for small metazoans and bacteria (Levin and Gooday, 1992). The large foraminiferan xenophyophores are the most abundant group in polymetallic nodule fields identifiable at the megabenthic scale (Rodrigues et al., 2001; Amon et al., 2016), but live specimens cannot be distinguished from dead specimens (Hughes and Gooday, 2004) from imagery.

The limited DCF and xenophyophore data available for the DEA were combined with literature data and some assumptions, which resulted in resolvable, but poorly constrained, adjustments of the presented food-web models (Appendix, Table A6). This inclusion of DCF and xenophyophores did not result in changes to our conclusions (Table A7). The addition of xenophyophores was possible within the same C influx into the system but resulted in a significantly higher *T*.. and *FCI* for all sites (Table A7). This can be interpreted as increased recycling of C that can sustain an increase in biomass even though food availability stays the same.

Carcasses, or carrion, are bulky detritus resources which are easily accessible by larger fauna, but also experience microbial degradation. The importance of microbial degradation of abyssal carcasses is poorly studied, and thus microbial degradation of carcasses is currently not included in the food-web model. The scavenging rate on abyssal carcasses is very high (e.g. Harbour et al., 2020) and thus the microbial contribution to carcass C cycling might be negligible. However, microbes are able to access particular carcass components that are often not edible by scavengers (e.g. bones, Smith et al., 2015) and may influence the scavenging rate (e.g Burkepile et al., 2006), thus these food-web interactions are an interesting avenue for further research.

The reference site was assumed to not have been impacted by the experimental disturbance, but no pre-disturbance data have been collected there. The representativeness and hence the use of reference sites as an experimental control with regard to the DEA has been called into question (Simon-Lledó et al., 2019b). Large-scale temporal differences that affect the benthic system like fluctuations in detritus deposition (Bluhm, 2001) are expected to influence all sites evenly as they were sampled in the same year and season. However, small-scale spatial variations in environmental conditions of nodule fields may explain part of the observed differences between the experimental and reference areas, which were located 4 km apart. Significant variation in faunal and prokaryotic communities on the abyssal plains have been demonstrated at spatial scales of <1 km (Janssen et al., 2015), <10 km (Simon-Lledó et al., 2019b), and <60 km (Molari et al., 2020). A rough estimate of nodule density and weight based on box core data (Greinert, 2015) shows that at the experimental site (n = 14) the nodule density (8.4 ± 6.4 nodules m^{-2}) and weight (5.6 ± 4.0 kg nodules m^{-2}) appears to be lower than at the reference site (29 ± 15 nodules m^{-2} and 14 ± 8.0 kg nodules m^{-2}, n = 10), which might explain part of the observed differences (De Smet et al., 2017; Simon-Lledó et al., 2019b; Vanreusel et al., 2016). Understanding the natural spatial variation of abyssal communities is a major knowledge gap, and should be addressed in order to better interpret the outcome of disturbance studies (Gollner et al., 2017).

4.2. Long-term effects of abyssal sediment disturbance on carbon cycling

The presented food-web models allowed us to estimate C fluxes that could not be measured *in situ,* and to assess the long-term effects of a small-scale benthic disturbance on abyssal C cycling. Our main findings are that inside the plough tracks overall modelled faunal respiration appears to have recovered to and sometimes exceeded reference values 26 years after the initial disturbance, although there was variation among food-web compartments, whereas the microbial loop and consequently the total system C flow is still impaired (Table 6). This section discusses these results in light of previous disturbance studies and in the greater context of abyssal system functioning.

Our modelling exercise showed that overall faunal respiration was significantly higher inside the plough tracks compared to the reference sites, and not significantly different between outside and inside the plough tracks (Table 6). A review of previous disturbance studies showed a general trend that small mobile fauna generally recovered faster than larger sessile fauna, sometimes even exceeding pre-disturbance abundances, although the extent of recovery was highly variable among taxonomic groups and locations (Gollner et al., 2017; Jones et al., 2017). This study also found variability in recovery among different faunal food-web compartments, with two-thirds of the faunal compartments having a higher respiration rate, and one-third exhibiting lower respiration rates inside the plough track compared to the reference site. In line with the reviewed studies, we observed a general trend of recovered respiration in metazoan meiofauna, sometimes greatly exceeding reference values (up to a 927% for respiration of omnivorous and predatory nematodes), whereas macrofaunal respiration was similar to, or smaller than reference values (Tables 6 and 7).

Perhaps unexpectedly, overall megafauna respiration inside the plough tracks was significantly higher at the experimental compared to the reference sites (Table 6), with the notable exception of holothurians (in contrast to Simon-Lledó et al., 2019b; Stratmann et al., 2018c) and *Ipnops* sp. (in line with Simon-Lledó et al., 2019b). Although the modelled holothurian respiration rate is significantly reduced at the experiment site, i.e. the model finds reduced holothurian respiration in at least 95% of all model outcomes, the absolute differences in respiration between sites (range from 2.91×10^{-4} to 3.56×10^{-4} mmol C m^{-2} d^{-1}) are relatively small compared to the range of holothurian respiration rates found by Stratmann et al. (2018c) (4.5×10^{-4}–10.6×10^{-4} mmol C m^{-2} d^{-1}). Stratmann et al. (2018c) concluded that holothurian density and respiration had recovered when compared to historical density values at the DEA. At first glance, the relatively high faunal C cycling in the plough tracks does not appear to concur with the reduction in bioturbation activity found by Vonnahme et al. 2020. However, the extent of bioturbation directly scales with organism size (Middelburg, 2019), and we found that macrofauna in contrast to meiofauna had reduced respiration inside the plough tracks.

Our finding that overall faunal respiration had recovered is in stark contrast to the conclusions of Stratmann et al. (2018a) who found significantly reduced faunal respiration inside the plough tracks 26 years after the initial disturbance compared to outside the plough tracks (Stratmann et al., 2018a). This difference in findings results from the improved resolution of the food-web model and biomass estimation methods. First of all, while the study by Stratmann et al. (2018a) only incorporated macrofauna and megafauna in the model, this study additionally included metazoan meiofauna. Our models estimated that metazoan meiofauna strongly dominated C ingestion (Fig. 4) and overall faunal respiration (Table 7). Therefore, the reduced metazoan meiofaunal respiration at the reference site compared to the experimental

sites largely explains the different conclusions in the present study and in Stratmann et al. (2018a). Nevertheless, when only taking macrofauna and megafauna respiration into account, we did not find the inside and outside plough tracks to be significantly different (Table 6) in contrast to Stratmann et al. (2018a). This is remarkable as identical macrofauna and megafauna density datasets were used in Stratmann et al. (2018a) and this study. However, Stratmann et al. (2018a) compared several food webs over a time range spanning 26 years, and was therefore restricted to include only those macrofaunal taxa that were consistently quantified, resulting in exclusion of several taxa that were investigated in 2015, but not in previous years. Additionally, the individual biomasses of megafauna estimated by Stratmann et al. (2018a) were based on a relatively coarse taxonomic resolution predefined by Bluhm (2001). For the present study, we identified megafauna to the highest taxonomic resolution possible, and calculated individual biomasses using conversion factors with the same resolution. Hence, megafaunal C stocks presented in this study are more precise than the megafaunal stocks reported in Stratmann et al. (2018a).

Differences in the summed C flows (*T*..) among reference sites and inside plough tracks, and among outside and inside plough tracks were mainly the result of significant differences in the microbial loop (Fig. 5). Both prokaryotic biomass and C production inside plough tracks were lower compared to reference sites, although the microbial community structure after 26 years was not significantly different between the reference and experimental sites (Vonnahme et al., 2020). The apparent slow recovery of prokaryotic C cycling is remarkable, since bacteria are generally considered to have relatively short generation times and high growth rates even in abyssal sediments (Deming, 1985; Jørgensen and Boetius, 2007). Abyssal prokaryotic communities are strongly linked to sediment geochemistry, as illustrated by the significant change in prokaryotic density (Deming, 1985), C production rates (Luna et al., 2013), and community composition with depth (Lindh et al., 2017; Shulse et al., 2017) and polymetallic nodule abundance (Tully and Heidelberg, 2013; Lindh et al., 2017; Cho et al., 2018; Molari et al., 2020). Although most, but not all, porewater profiles at the DISCOL sites were fully regenerated after 26 years, differences in the solid phase profiles were still clearly visible between undisturbed and disturbed sediments (Paul et al., 2018). This was confirmed by Vonnahme et al. (2020) who found that altered sediment integrity and biogeochemistry inside the plough tracks was related to strongly reduced prokaryotic growth efficiencies and extracellular enzymatic activity. It is important to note that for constructing our food-web model for inside the plough track we omitted the microhabitat 'sub-surface patch' and aggregated the microhabitats 'plough furrows' and 'plough ridges' as defined in Haffert et al. (2020), Paul et al. (2018), and Vonnahme et al. (2020). In contrast, these DEA sediment biogeochemistry studies (Haffert et al., 2020; Paul et al., 2018; Vonnahme et al., 2020) specifically looked at the separate microhabitats and found biogeochemical differences even among the plough track microhabitats, with subsurface patches often being the most impacted.

Outside the plough tracks, the effects of the original sediment disturbance are expected to be limited to sedimentation of resuspended particles as the sediment integrity was kept intact. Indeed, the modelled food-web characteristics outside the plough tracks are a mixture of characteristics either similar to the reference site model or inside the plough tracks model. Just like inside the plough tracks, estimated prokaryotic and therefore overall respiration outside the plough tracks was significantly lower compared to the reference site. In contrast, the microbial loop, which includes microbial respiration, outside the plough track was not significantly different compared to the reference site. Additionally, outside the plough tracks total modelled C throughput *T*.. was higher, although not significantly, than at the reference site. Also faunal respiration and Finn's Cycling Index *FCI* were significantly higher outside the plough tracks. The high C cycling and recycling efficiency outside the plough tracks are therefore likely related to changes in the faunal community rather than the prokaryotic community. The mechanism behind increased faunal cycling possibly linked to settling resuspended sediment is unknown, as the effects of plume forming and consequent increased sedimentation in areas adjacent to deep-seabed mining have not yet received elaborate attention (Drazen et al., 2020), but may be related to input of new nutrients and carbon originating from deeper sediment layers of the ploughed area (Raghukumar et al., 2001; Sharma et al., 2001).

The impaired microbial loop did not appear to affect abyssal faunal C cycling in this study. This is consistent with the finding that C transfer from microbes to deep-sea metazoans in deep-sea sediments is rather inefficient. For instance, there was no significant transfer of C derived from bacteria to metazoan consumers in sediments of the Arabian Sea (Pozzato et al., 2013; Middelburg, 2018). However, for fauna feeding on prokaryotes the model does show a diet shift with reduced feeding on prokaryotes and a greater importance of feeding on detritus, notably semi-labile detritus (Fig. 4). This diet shift is also visible for xenophyophores when added to the model (Table A7). So, although overall faunal C cycling was not significantly impacted, the importance of food source was shifted away from the microbial community towards deposited detritus.

The models did not reveal any indications of reduced system complexity due to species mortality or significantly altered trophic-chain lengths due to the sediment disturbance. The average number of links per food-web compartment (*LD*) was similar in- and outside the plough tracks and only slightly lower at the reference sites. The total fraction of realised links (*C*) shows small increases in connectance from inside to outside the plough tracks to reference sites (Table 5). No significance value can be calculated for *LD* and *C* as they are based on network topology which is the same in every model solution. However, a decline in *C* with a larger number of food-web compartments when *LD* remains constant is inherent to the calculation of these network indices (Pimm et al., 1991), suggesting the differences in C between sites are not of important magnitude. As these complexity indices are sensitive to compartment resolution, the results may be different if the food-web is resolved to species level.

The maximum trophic level (*TL*) in a food web is significantly related to resource availability under very low food input (<10 g C m^{-2} y^{-1}), but in a non-linear relationship where intermediate availability, not the highest, results in the longest trophic chains (Post, 2002). Maximum *TL* did not significantly differ between sites, and thus resource availability and the efficiency of C transfer to higher trophic levels do not appear to be affected by the sediment disturbance. Although the differences in *TL* were not significant, it is likely that the maximum *TL* inside the plough tracks is highest due to the greater biomass of scavengers and fish, and the low mean *TL* inside the plough tracks is caused by the reduced importance of grazing on prokaryotes (Fig. 4).

The extent of C cycling by fauna and in the microbial loop at all three sites was comparable to C cycling in other abyssal plain systems. Carbon cycling was modelled in previous studies for two other abyssal plain systems both considered eutrophic systems influenced by seasonal pulses of POC (Rice et al., 1994; Smith and Druffel, 1998): Station M located in the abyssal North-East Pacific (Dunlop et al., 2016) and the lesser eutrophic Porcupine Abyssal Plain (PAP) in the North-East Atlantic (van Oevelen et al., 2012; Durden et al., 2017). The Peru Basin is known to experience relatively high fluxes of organic matter compared to other abyssal plains due to its location near the equatorial zone of high productivity and is also considered eutrophic (Smith et al., 1996, 1997). Community respiration at the Peru Basin reference site (0.78 mmol C m^{-2} d^{-1}) was similar to community respiration estimated by the food-web model of Station M (0.71–0.74 mmol C m^{-2} d^{-1}) (Dunlop et al., 2016). In contrast, community respiration inside plough tracks (0.59

mmol C m^{-2} d^{-1}) was similar to the community respiration at PAP (0.45–0.56 mmol C m^{-2} d^{-1}) (van Oevelen et al., 2012; Durden et al., 2017). The contribution of prokaryotic respiration was consistently between 70% and 92% of total community respiration in all models, including this study, highlighting the importance of the prokaryotic community for abyssal plains (Rowe and Deming, 1985; Lochte and Turley, 1988; Boetius and Lochte, 1996; Sweetman et al., 2019). The size of prokaryotic processes (sum of detritus dissolution, DOC uptake, and respiration) was similar between Station M (1.8–2.2 mmol C m^{-2} d^{-1}) (Dunlop et al., 2016) and the Peru Basin (1.9–2.8 mmol C m^{-2} d^{-1}), with lower reported values at PAP (1.2–1.3 mmol C m^{-2} d^{-1}) (van Oevelen et al., 2012; Durden et al., 2017).

4.3. Outlook to deep-seabed mining effects

The DISCOL experiment covered an area of 11 km^2 (Thiel et al., 1989), whereas industrial-scale seabed mining activity is expected to affect an area at least one to two orders of magnitude larger. Based on our results, we can assume that industrial-scale polymetallic nodule extraction will impair the microbial loop. Our results highlight the key role of the microbial community in benthic C cycling at abyssal depths as shown in other deep-sea studies (Rowe and Deming, 1985; Lochte and Turley, 1988; Boetius and Lochte, 1996; Sweetman et al., 2019) and the fact that deep-seabed mining will in all likelihood modify the processes these key organisms carry out. However, faunal recovery rates for industrial-scale seabed mining activity cannot directly be extrapolated from small-scale disturbance results, because ecosystem recovery in a commercial mining context will be dependent on a variety of factors, including, but not limited to large-scale dispersal, connectivity, re-colonisation, and the availability of C in subsurface sediments exposed by mining machines. Faunal recovery may partly be facilitated by recruitment from unaffected adjacent areas, but this process might be slowed in mined areas with reduced connectivity to these unaffected areas.

Additionally, the DISCOL experiment did not remove nodules from the seafloor but ploughed them below the sediment surface. The removal of nodules, which will occur during industrial exploitation, will destroy nodule-obligate fauna and change the community composition, especially the presence of sessile species like corals, sponges, and xenophyophores (Simon-Lledó et al., 2019a, 2019b; Vanreusel et al., 2016). Even though a change in community composition is likely to result in an observable change in C cycling, it is theoretically possible that ecosystem functioning in terms of C cycling is the same between varying community compositions which differ when reviewed for another type of function, like the degree of habitat forming structures. Therefore, diversity indices should be reviewed alongside ecosystem functioning.

Finally, it is important to note that deep-seabed mining is only a single stressor potentially affecting abyssal systems. Other anthropogenically induced changes, most importantly climate change (Sweetman et al., 2017), will also exert stress on abyssal ecosystems with potentially unknown synergistic effects (Ramirez-Llodra et al., 2011). Our model results show that fauna can shift towards a more detritus-based diet when the prokaryotic community is impaired due to deep-seabed mining, and we could speculate that this increased faunal demand for high-quality detritus cannot be met under future climate scenarios. In future abyssal climate scenarios the C demand will be higher due to increased metabolic rates with higher temperatures, but the detritus deposited on abyssal sediments will likely be of lower quantity and quality (Sweetman et al., 2017). Therefore, besides scaling predicted effects from mining simulations to industrial scale mining, policy should also take into account the additional effects of biogeochemical changes due to climate change, resource exploitation, and other human activities on abyssal ecosystems.

5. Conclusion

Based on the most highly resolved deep-sea food-web model to date, both in food-web complexity and data availability, we show that 26 years after a small-scale sediment disturbance total C throughput was 16% lower, and microbial loop C cycling was reduced by 35% inside plough tracks compared to reference sites. This indicates that ecosystem functioning in terms of C cycling had not recovered from the disturbance, and that the microbial loop was still impaired. Faunal respiration recovered to, and exceeded reference values but varied among faunal compartments. Recovery of the prokaryotic community was most likely closely related to recovery of sediment integrity and biogeochemistry, so sediment integrity and prokaryotic production could be used as an extra environmental proxy for monitoring abyssal ecosystems, besides faunal monitoring. The impaired microbial loop observed at DISCOL is expected to also occur if large-scale polymetallic nodule mining commences, which could affect ocean biogeochemistry. The importance of taking into account the effects of deep-seabed mining on the microbial-mediated biogeochemical processes is also highlighted by Orcutt et al. (2020). Additional incorporation of xenophyophore and DCF processes in the DISCOL food-web models, though based on severely limited data, confirms overall conclusions and highlights the potentially great importance of these components in abyssal C cycling. Future research into these poorly understood biogeochemical processes at the base of the food web is therefore highly recommended. It is difficult to predict if faunal carbon-flow recovery rates will be the same following industrial-scale seabed mining over prolonged periods of time, due to potentially less recruitment possibilities in affected areas and synergistic effects with other anthropogenically-induced stressors, such as climate change. Resolved food-web models, like the ones presented, can potentially be employed to construct dynamic models (e.g. *sensu* van Oevelen et al., 2012) to study ecosystem stability and predict future changes by altering constraints and forcing flows based on e.g. climate predictions. This study shows mining of polymetallic nodules will likely reduce ecosystem functioning on at least decadal time scales.

Declaration of Competing Interest

The authors declare that they have no known competing financial interests or personal relationships that could have appeared to influence the work reported in this paper.

Acknowledgements

The research leading to these results has received funding from the European Union Seventh Framework Programme (FP7/2007–2013) under the MIDAS project, grant agreement no 603418 and by the JPI Oceans – Ecological Aspects of Deep Sea Mining project (NWO-ALW grant 856.14.002)), by the JPI Oceans – Impacts of deep-sea nodule mining project “MiningImpact 2” (NWO-ALW grant 856.18.003), and the Bundesministerium für Bildung und Forschung (BMBF) grant n° 03F0707A-G. Additional financial support was granted to CESAM (UID/AMB/50017 – PO-CI-01-0145-FEDER-007638), to FCT/MCTES by national funds (PIDDAC), and by co-funding by the FEDER, within the PT2020 Partnership Agreement and Compete 2020. CFR was supported by Fundação para a Ciência e a Tecnologia (FCT) grant (SFRH/BPD/107805/2015). DvO and TS were also supported by the Dutch Research Council (DvO: NWO-VIDI grant no. 864.13.007, TS: NWO-Rubicon grant no. 019.182EN.012).

Appendix A

This appendix contains additional information and data used to construct the food-web inverse models.

Table A1
Feeding types and taxon-specific biomasses (mmol C ind^{-1}) of all metazoan meiofauna included in the food-web models. Abbreviations are: MeiB = metazoan meiofauna bacterivores, MeiDF = metazoan meiofauna deposit feeders, MeiFSF = metazoan meiofauna filter and suspension feeders, MeiP = metazoan meiofauna predators, MeiOF = metazoan meiofauna omnivores, NemNSDF = nematode non-selective deposit feeders, NemEF = nematode epistrate feeders, NemOP = nematode omnivores and predators; REF = reference sites, OPT = outside plough tracks, IPT = inside plough tracks. References for feeding types (Ref.): [1]Giere (2009), [2]Fox et al. (2003), [3]Enríquez-García, Nandini and Sarma, (2013), [4]McClain, Johnson and Rex (2004), [5]Menzies (1962), [6]Heiner, Vinther Sørensen and Møbjerg Kristensen (2018), [7]Miljutin et al. (2011), [8]Giere (2006), [9]Stratmann et al. (2018a). References for biomasses: [10]Stratmann et al. (2018b), [11]Galéron et al. (2000), [12]Zeng et al. (2018), [13]Bianchelli et al. (2010), [14]Rex et al. (2006).

Taxon	Feeding type	Biomass	Ref.
Bivalvia[a]	MeiFSF	3.48×10^{-5}	1, 2, 13
Cyclopoida	50% MeiOF, 50% MeiP	5.97×10^{-7}	1, 3, 11
Gastropoda[c]	90% MeiDF, 10% MeiP	1.59×10^{-5}	4, 13
Gastrotricha[b]	MeiB	5.96×10^{-7}	1, 13
Harpacticoida	MeiDF	7.01×10^{-5}	1, 2, 11
Isopoda[a]	93% MeiDF, 7% MeiP	1.24×10^{-4}	5, 13
Kinorhyncha[a]	50% MeiB, 50% MeiDF	4.22×10^{-6}	1, 2, 13
Loricifera[c]	MeiB	1.59×10^{-5}	6, 14
Nematoda	50% NemNSDF, 25% NemEF, 25% NemOP	2.97×10^{-6}	7, 10
Oligochaeta[a]	MeiDF	9.43×10^{-5}	8, 13
Ostracoda	MeiOF	4.98×10^{-4}	1, 12
Polychaeta	REF: 54% MeiDF, 13% MeiFSF, 23% MeiP, 10% MeiOF; OPT: 50% MeiDF, 17% MeiFSF, 18% MeiP, 15% MeiOF; IPT: 58% MeiDF, 19% MeiFSF, 17% MeiP, 6% MeiOF	1.48×10^{-4}	9, 12
Rotifera[c]	MeiDF	1.59×10^{-5}	1, 14
Tanaidacea[b]	MeiOF	1.18×10^{-5}	1, 13
Tardigrada[b]	MeiB	1.05×10^{-7}	1, 13

[a] Taxon-specific individual biomasses for abyssal plains (B_{4000}; mmol C ind^{-1}) were calculated as $B_{4000} = 10^{log_{10}(B_{1887}) - \beta_{meiofauna} \times \Delta depth}$, where B_{1887} corresponds to the taxon-specific individual biomass (mmol C ind^{-1}) from the southern open slope of the Catalan Margin (1887 m depth; NW Mediterranean Sea) (Bianchelli et al., 2010). $\beta_{meiofauna}$ (=1.70×10^{-4}) corresponds to β in the regression analysis for meiofauna biomass in Rex et al. (2006) and Δdepth is the depth difference between the abyssal plains (~4,000 m depth for the DISCOL experimental site) and the slope station (1,887 m depth).

[b] Taxon-specific individual biomasses for abyssal plains (B_{4000}; mmol C ind^{-1}) were calculated as $B_{4000} = 10^{log_{10}(B_{985}) - \beta_{meiofauna} \times \Delta depth}$, where B_{985} corresponds to the taxon-specific individual biomass (mmol C ind^{-1}) from the southern open slope of the Catalan Margin (985 m depth; NW Mediterranean Sea) (Bianchelli et al., 2010) and Δdepth is the depth difference between the abyssal plains (~4,000 m depth for the DISCOL experimental site) and the slope station (985 m depth).

[c] The individual biomass corresponds to the mean biomass of an individual deep-sea meiofaunal organisms at 4,100 m depth (Rex et al., 2006).

Feeding types and taxon-specific biomasses

The feeding types and taxon-specific biomasses used to calculate the C stocks for the different food-web compartments are given in Tables A1, A2, A3, and A4

Table A2
Feeding types of all metazoan macrofauna included in the food-web models. The taxon-specific individual biomass data (mmol C ind^{-1}) were taken from Stratmann et al. (2018a). Abbreviations are: MacDF = macrofauna deposit feeders, MacFSF = macrofauna filter and suspension feeders, MacOF = macrofauna omnivores, MacP = macrofauna predators, PolSDF = polychaete surface deposit feeders, PolSF = polychaete suspension feeders, PolSSDF = polychaete subsurface deposit feeders, PolP = polychaete predators, PolOF = polychaete omnivores; REF = reference sites, OPT = outside plough tracks, IPT = inside plough tracks. References for feeding types (Ref.): [1]Gage and Tyler (1991), [2]WoRMS Editorial Board (2019), [3]Fox et al. (2003), [4]Smith and Stockley (2005), [5]McClain, Johnson and Rex (2004), [6]Menzies (1962), [7]Iken et al. (2001), [8]Jumars, Dorgan and Lindsay (2015), [9]Vannier, Abe and Ikuta (1998), [10]Gowing and Wishner (1986).

Taxon	Feeding type	Biomass	Ref.
Amphipoda	50% MacOF, 50% MacP	3.68×10^{-3}	1, 2
Bivalvia	MacFSF	1.41×10^{-3}	3
Copepoda	MacDF	5.39×10^{-4}	10
Cumacea	MacDF	3.09×10^{-3}	3
Echinoidea	85% MacOF, 15% MacDF	9.66×10^{-3}	4
Gastropoda	90% MacDF, 10% MacP	8.56×10^{-2}	5
Isopoda	93% MacDF, 7% MacP	1.33×10^{-3}	6
Nematoda[a]	75% MacDF, 25% MacP	3.26×10^{-4}	9
Ophiuroidea	MacDF	9.66×10^{-3}	7
Ostracoda	MacOF	2.27×10^{-3}	3
Polychaeta	REF: 13% PolSF, 38% PolSDF, 16% PolSSDF, 23% PolP, 10% PolOF; OPT: 17% PolSF, 37% PolSDF, 13% PolSSDF, 18% PolP, 15% PolOF; IPT: 19% PolSF, 42% PolSDF, 16% PolSSDF, 17% PolP, 6% PolOF	1.33×10^{-2}	8
Scaphopoda	MacP	9.66×10^{-3}	3
Tanaidacea	MacDF	5.48×10^{-3}	3

[a] Macrofauna nematodes were divided into feeding types following the feeding type classification for meiofauna nematodes.

Sampling regime

The sampling regime, i.e. location, used sampling gear, and sample size, to determine site-specific parameters are given in Table A5.

Protozoa and DCF

The omission of protozoa and dark carbon fixation from the food-web model is a limitation that needs to be discussed. To aid this discussion, the limited site-specific data on these two food-web components that were available were additionally incorporated into the model to observe the effect on the overall food-web solution. The method is outlined below, and the additional site-specific parameters are presented in Table A6.

For the DISCOL site only xenophyophore density data was available (REF = 0.488 ind m^{-2}, OPT = 0.396 ind m^{-2}, IPT = 0.169 ind m^{-2}), but no size annotations were performed. Image annotations of xenophyophores from the APEI6 area in the CCZ (Simon-Lledó et al., 2019a) did include size measurements, and the average test size was estimated at 31.09 ± 11.06 mm (n = 39337). Individual average test volume was estimated from this average size with the regression Test Volume (mL) = 2.311 * Test Size (cm) − 0.877 (R^2 = 0.71, n = 6) based on the data in Levin and Gooday (1992). Individual xenophyophore protoplasm

Table A3
Feeding types for megafauna specimen photographed with an "Ocean Floor Observatory System" in the Peru Basin (SE Pacific). Median taxon-specific individual biomass (mmol C ind^{-1}) was calculated as described in Stratmann, Lins et al. (2018) based on length measurements of individual organisms in the Peru Basin. *n* refers to the number of individuals used to estimate taxon-specific biomasses.

Abbreviations are: MegDF = megafauna deposit feeders, MegFSF = megafauna suspension and filter feeders, MegSDF = megafauna surface deposit feeders, MegSSDF = megafauna subsurface deposit feeders, MegP = megafauna predators, MegOF = megafauna omnivores, MegS = megafauna scavengers; REF = reference sites, OPT = outside plough tracks, IPT = inside plough tracks. References for biomasses (Ref.): [1]Stratmann et al. (2018c), [2]Tilot (1992), [3]Stratmann et al. (2018a), [4]Durden, et al. (2016), [5]Rex et al. (2006), [6]this study. References for feeding type (Ref.): [7]Fox et al. (2003), [8]Gage and Tyler (1991), [9]WoRMS Editorial Board (2019), [10]Menzies (1962), [11]Escobar-Briones et al. (2002), [12]MacAvoy et al. (2008), [13]Nakamura et al. (2015), [14]Smith and Stockley (2005), [15]McClain et al. (2004), [16]Bluhm (2001), [17]Fratt and Dearborn (1984), [18]Wigham et al. (2003), [19]Wigham et al. (2008), [20]Roberts et al. (2000), [21]Iken et al. (2001), [22]Billett et al. (2001), [23]Hudson et al. (2004).

Taxa	Feeding type	*n*	Biomass	Ref.
Annelida				
Polychaeta[a]	REF: 54% MegDF, 13% MegSF, 23% MegP, 10% MegOF; OPT: 50% MegDF, 17% MegSF, 18% MegP, 15% MegOF; IPT: 58% MegDF, 19% MegSF, 17% MegP, 6% MegOF	62	0.53	3
Arthropoda				
Amphipoda	50% MegP/ 50%MegS	8	3.58	6, 21
Cirripedia	MegFSF	2	176	6, 7
Isopoda	93% MegDF, 7% MegP	19	8.13	6, 10
Munidopsidae	MegDF	41	267	6, 21
Probeebei sp.	MegDF	421	68.3	6, 8
Pycnogonida	50% MegP, 50% DF	41	3.73	6, 8, 21
Other crustaceans	MegP	41	2.6	6, 8
Chordata				
Ascidiacea[b]	MegFSF		0.83	2, 7
Cnidaria				
Actiniaria	MegFSF	301	0.30	3, 7
Antipatharia	MegFSF	3	177	3, 7
Ceriantharia[b]	MegFSF		1923	2, 7
Gorgonaria	MegFSF		21.7	2, 7
Other Cnidaria[c]	MegFSF		0.24	6, 7
Echinodermata				
Asteroidea	50% MegDF, 50% MegP	53	139	3, 21
Crinoidea[b]	MegFSF		5.33	2, 7
Echinoidea[b]	15% MegDF, 85% MegOF		59.2	2, 14
Ophiuroidea	MegOF	527	16.1	3, 8
Holothurian morphotypes				
Abyssocucumis abyssorum	MegFSF	1	4.98	1, 7, 20
Amperima sp.	MegSDF	73	18.1	1, 7, 18, 21
Bathyplotes sp.[c]	MegSDF	552	7.48	1, 23
Benthodytes gosarsi	MegSDF	2	61.1	1, 7, 21
Benthodytes sp.	MegSDF	12	3.00	1, 7, 21
Benthodytes typica	MegSDF	123	22.7	1, 7, 21
Benthothuria sp.[c]	MegSDF	552	7.48	1, 23
Elpidiidae gen. sp.1	MegSDF	24	2.84	1, 22
Elpidiidae gen. sp. 2	MegSDF	15	11.0	1, 22
Elpidiidae gen. sp. 3	MegSDF	5	2.06	1, 22
Galatheathuria sp.	MegFSF	6	66.0	1, 22
Mesothuria sp.	MegSSDF	94	4.32	1, 7, 21
Oneirophanta sp.	MegSDF	11	9.99	1, 7, 21
Peniagone sp. (morphotype "palmata")	MegSDF	21	1.71	1, 7, 21
Peniagone sp. 1	MegSDF	21	3.27	1, 7, 19, 21
Peniagone sp. 2 (benthopelagic)[c]	MegSDF	552	7.48	1, 7, 19, 21
Psychronaetes hanseni[c]	MegSDF	552	7.48	1, 20
Psychropotes depressa	MegSDF	13	28.2	1, 7, 21
Psychropotes longicauda	MegSDF	9	4.44	1, 7, 21
Synallactidae gen. sp. 1[d]	MegSDF	26	2.41	1
Synallactidae gen. sp. 2[d]	MegSDF	46	2.10	1
Synallactes profundi[e]	MegSDF	17	2.46	1
Synallactes sp. (morphotype "pink")[c]	MegSDF	11	4.36	1
Unknown holothurians[c]	MegSDF	552	7.48	1
Hemichordata				
Hemichordata[e]	MegDF		22.4	5, 8
Mollusca				
Gastropoda[e]	90% MegDF, 10% MegP		22.4	6, 15
Porifera				
Porifera[b]	MegFSF		6.74	2, 7

[a] As no information about families and/or feeding types was available for megafauna polychaetes, the macrofauna polychaete feeding type composition was also used for the megafauna polychaete feeding type composition.

[b] Mean taxon-specific biomass data per individual were extracted from Tilot (1992) for the CCZ.

[c] The taxon-specific individual biomass of this holothurian morphotype is the mean biomass of all holothurians.

[d] As the gut content of a specimen of Synallactidae collected in the Peru Basin (Stratmann, unpublished data) showed an 18 times enrichment in organic C compared to surrounding sediment, all Synallactidae, *Synallactes profundi*, and *Synallactes* sp. were classified as surface deposit feeder.

[e] Individual biomass calculated for mean benthos megafauna at 4100 m depth based on the biomass-bathymetry and abundance-bathymetry relationships presented in Rex et al. (2006).

volume for the average test size was estimated with the regression Protoplasm Volume (mL) = 0.030 * Test Volume − 0.011 (R^2 = 0.86, n = 4) based on Micro-CT 3D imaging data from Gooday et al. (2018). The density of xenophyophores at the three sites as calculated from the annotations combined with the individual protoplasm volume was used to estimate xenophyophore biomass (mmol C m^{-2}) by assuming 1.02 g protoplasm wet weight per mL protoplasm (Snider et al., 1984) and 0.1 g C per g protoplasm wet weight (Gerlach et al., 1985; Korsun et al., 1998). Assuming all observed xenophyophores were alive, this results in a biomass of 0.25 (IPT) to 0.73 (REF) mmol C m^{-2} (Table A6). This biomass does not include any associated prokaryotes or metazoans.

Xenophyophores that were added to the model fed on labile and semi-labile detritus from the sediment and from suspension (Levin, 1991; Levin and Gooday, 1992; Gooday et al., 2020), on bacteria (Laureillard et al., 2004; Mojtahid et al., 2011), and on labile DOC (DeLaca et al., 1981; Nomaki et al., 2011). No feeding selectivity was assumed. Xenophyophores are preyed upon by macrofaunal (incl. polychaetes) and megafaunal (surface) deposit feeders (incl. holothurians), omnivores, and predators (except fish) (Levin, 1991; Levin and Gooday, 1992; Gooday et al., 2020). Faecal pellets of xenophyophores are called stercomata, and are assumed to be semi-labile and refractory. Mortality of xenophyophores results in semi-labile detrital material.

Secondary production of xenophyophores *SP* was based on the slowest and fastest observed increases in test volume over time (Gooday et al., 1993) and *R* was based on minimum and maximum reported benthic foraminiferal respiration reported by Nomaki et al. (2007), Piña-Ochoa et al. (2010), Geslin et al. (2011) (Table A6). As assimilation efficiency has never been determined for xenophyophores or any other Foraminifera, the smallest minimum and the largest maximum *AE* constraints for metazoan invertebrate benthos from Table 3 were estimated. *NGE* for xenophyophores was estimated using Eq. (7) and the *SP* and *R* rates. Unfortunately, this mixture of physiological constraints was not compatible with the model, and only the upper constraint for production rate was used.

Prokaryotic DCF rates were determined by Vonnahme et al. (2020) through the addition of ^{14}C-labelled bicarbonate to sediment

Table A4
Diet, fish taxon-dependent conversion factors, and median taxon-specific individual biomass (mmol C ind^{-1}) of all fish specimens that were observed on pictures taken with the "Ocean Floor Observatory System" in the Peru Basin. *n* refers to the number of individuals used to estimate taxon-specific biomasses. Abbreviations are: REF = reference sites, OPT = outside plough tracks, IPT = inside plough tracks. References for feeding types: [1]Crabtree et al. (1991), [2]Drazen and Sutton (2017), [3]Sulak et al. (1985), [4]Gerringer et al. (2017).

Diet	Conversion factors[a]				*n*	Biomass
	a	*b*	Dry weight/ wet weight	C/dry weight		
Bathysaurus mollis[1,2,3]						
0–1.6% MegFSF, 11.2–12.5% MegDF, 0.2–2.4% MegP, 0.01–0.02% MegS, 43–100% *Ipnops* sp., 43–100% Ophidiidae, 0.2% carrion	3.24×10^{-3}	3.16	0.24	0.42	2	OPT: 6,715 IPT: 21,114
Ipnops sp.[1,2]						
3–6% MegFSF, 28.8–79.8% MegDF, 13.1–64.7% MegP, 3.5–6.6% MegS	4.90×10^{-3}	3.03	0.24	0.42	10	REF: 64.1 OPT: 108 IPT: 87.4 ± 0.29
Ophidiidae[1,2,4]						
0.3–0.6% MegFSF, 28.7–79.6% MegDF, 13–64.6% MegP, 3.5–6.6% MegS, 0.2% carrion	1.02×10^{-3}	3.06	0.17	0.38	3	OPT: 154 IPT: 720 ± 675; 720

[a] Length *L* (cm) of each specimen was measured in PAPARA(ZZ)I (Marcon and Purser, 2017) using a unilateral triangle of laser points as reference (see also Stratmann et al. (2018c). This length measurement was converted to wet-weight *WW* (g ww ind^{-1}) following Froese, Thorson and Reyes (2014): $WW = a \times L^b$, where *a* and *b* are taxon-dependent conversion factors and subsequently to individual biomass (mmol C ind^{-1}) using conversion factors from Brey et al. (2010).

Table A5
Geographic location (GPS in latitude, longitude) and number (n) of the samples taken to determine various sample parameters at reference sites (REF), outside plough tracks (OPT), and inside plough tracks (IPT), including specification of the employed sampling gear. References (Ref.): [1]Haffert et al. (2020), [2]Vonnahme et al. (2020), [3]This study, [4]Stratmann et al. (2018b).

	REF		OPT		IPT			
Sample parameter	GPS	n	GPS	n	GPS	n	Sampling gear	Ref.
Sediment porosity[a]	−7.125°N, −88°451°E	1	−7.073°N, −88.464°E	1	−7.073°N, −88.464°E	1	Multi corer, push corer	1
	−7.076°N, −88°526°E	1	−7.074°N, −88.449°E	1	−7.074°N, −88.464°E	1		
	−7.101°N, −88°414°E	1	−7.078°N, −88.458°E	1	−7.075°N, −88.449°E	2		
			−7.078°N, −88.457°E	1	−7.078°N, −88.458°E	1		
Labile detritus	−7.076°N, −88.526°E	3	−7.075°N, −88.449°E	3	−7.074°N, −88.464°E	6	Push corer	2
	−7.083°N, −88.469°E	3	−7.078°N, −88.457°E	3	−7.075°N, −88.449°E	3		
	−7.101°N, −88.414°E	3	−7.074°N, −88.464°E	3	−7.079°N, −88.457°E	6		
					−7.075°N, −88.449°E	3		
Semi−labile detritus	−7.125°N, −88.450°E	1	−7.083°N, −88.470°E	1	−7.083°N, −88.470°E	1	Push corer, benthic lander	3
	−7.800°N, −88.270°E	2	−7.074°N, −88.449°E	1	−7.074°N, −88.449°E	1		
Refractory detritus[a]	(see Labile detritus)	9	(see Labile detritus)	9	(see Labile detritus)	18	Push corer	2
Prokaryotes	(see Labile detritus)	9	(see Labile detritus)	9	(see Labile detritus)	18	Multi corer, push corer	2
Metazoan meiofauna	−7.126°N, −88.450°E	2	−7.073°N, −88.463°E	3	−7.078°N, −88.457°E	6	Push corer	3, 4
			−7.075°N, −88.448°E	3	−7.075°N, −88.448°E	6		
					−7.073°N, −88.463°E	6		
Macrofauna	−7.126°N, −88.451°E	2	−7.074°N, −88.464°E	3	−7.074°N, −88.464°E	3	Box corer	3
	−7.126°N, −88.450°E	3	−7.074°N, −88.465°E	1				
	−7.076°N, −88.526°E	3	−7.075°N, −88.449°E	3				
	−7.077°N, −88.526°E	2						

[a] For the analysis of sediment porosity, labile detritus, refractory detritus, and prokaryotes, sediment samples were taken of the microhabitats "plough track furrow" and "plough track ridge".

Table A6
Additional site-specific parameters later incorporated to the inverse food-web models (i.e. not included in the main model presented in the manuscript) to aid in the discussion of model limitations. Detailed methods are outlined in the Appendix. Abbreviations are: *AE* = Assimilation Efficiency, *NGE* = Net Growth Efficiency, *SP* = Secondary Production, *M* = Mortality, *R* = Respiration. References: [1]Levin and Gooday (1992), [2]Gooday et al. (2018), [3]Snider et al. (1984), [4]Gerlach et al. (1985), [5]Korsun et al. (1998), [6]This study, [7]Gooday et al. (1993), [8]Nomaki et al. (2007), [9]Piña-Ochoa et al. (2010), [10]Geslin et al. (2011), [11]Vonnahme et al. (2020).

Model component	Parameters	Reference
Xenophyophore C stock, assuming 100% alive (mmol C m^{-2})	REF: 0.730 OPT: 0.592 IPT: 0.252	1, 2, 3, 4, 5, 6
Xenophyophore *AE* (-)[b]	[0.18, 0.89]	6
Xenophyophore *NGE* (-)[b]	[0.17, 0.76]	6
Xenophyophore *SP* (mmol C m^{-2} d^{-1})[b]	[1.30, 1.32] × C stock	7
Xenophyophore *M* (mmol C m^{-2} d^{-1})	[0, 1.32] × C stock	7
Xenophyophore *R* (mmol C m^{-2} d^{-1})[b]	[0.41, 6.36] × C stock	8, 9, 10
DIC to Prokaryotes[a] (mmol C m^{-2} d^{-1})	REF: [3.23 × 10^{-2}, 4.50 × 10^{-2}] OPT: [2.05 × 10^{-2}, 3.76 × 10^{-2}] IPT: [1.56 × 10^{-2}, 2.77 × 10^{-2}]	11
DIC-derived viral lysis of prokaryotes to DOC[a] (mmol C m^{-2} d^{-1})	REF: [8.11 × 10^{-2}, 1.06 × 10^{-1}] OPT: [7.30 × 10^{-2}, 8.63 × 10^{-2}] IPT: [2.61 × 10^{-2}, 8.68 × 10^{-2}]	11

[a] To calculate the flux IPT, the microhabitats "plough track furrow" and "plough track ridge" as defined in Vonnahme et al. 2020 were combined. The lower and upper constraints represent the first and third quartile of the dataset respectively.

[b] These constraints were dropped (except for the upper limit of *SP*) when the compatibility of the constraints in the model were checked. They are kept in this table to be able to compare them to the estimated physiological parameters based on the model fluxes as presented in Table A7.

incubations, and subsequent measurements of incorporation into DOC and prokaryotic biomass. DCF rates from the upper 1 cm for each site were converted from nmol C g^{-1} d^{-1} to mmol C m^{-2} d^{-1} using the sediment dry bulk density and surface porosity values reported in the main Materials & Methods section of the manuscript (IPT corresponded to the microhabitats 'Furrow' and 'Ridge' combined). The first and third quartile of DCF rates for each site based on the upper 1 cm were used as lower and upper constraints (Table A6). DCF rates could not be extrapolated to 5 cm, as DCF depth profiles were only available for three disturbed sites and no other data on DCF depth profiles is known. Therefore, the DCF rates used as constraints are underestimations. It was assumed that the uptake of DIC by prokaryotes leads to effective prokaryotic biomass production and is part of, not in addition to, prokaryotic production as estimated from ^{3}H-leucin incorporation. Furthermore, it was assumed that all DOC production from DIC comes from prokaryotic viral lysis.

The additional DISCOL food-webs for all three sites which now include xenophyophores and DCF were sampled 10,000 times, to reduce calculation times compared to the 100,000 iterations to resolve the main model. Assessment of all 10,000 solutions shows the required convergence and expected distributions, although with lower coverage than the main model. Results of some important food-web characteristics with a focus on xenophyophores and DCF are given in Table A7.

Table A7
Results for some main network characteristics for the DISCOL food-web model including DCF and xenophyophores as described in the Appendix. For fluxes the standard deviation is given. REF = reference sites, OPT = outside plough tracks, IPT = inside plough tracks. *T*.. = Total System Throughput, FCI = Finn's Cycling Index.

Model characteristic	REF	OPT	IPT
Total C inflow (mmol C m^{-2} d^{-1})	0.86 ± 3.32 × 10^{-2}	0.71 ± 3.35 × 10^{-2}	0.70 ± 3.53 × 10^{-2}
T.. (mmol C m^{-2} d^{-1})	6.42 ± 0.18	6.69 ± 0.28	5.15 ± 0.13
FCI (–)	0.35 ± 0.02	0.43 ± 0.02	0.29 ± 0.01
Total respiration (mmol C m^{-2} d^{-1})	0.77 ± 2.38 × 10^{-2}	0.61 ± 2.39 × 10^{-2}	0.59 ± 1.79 × 10^{-2}
Faunal respiration (mmol C m^{-2} d^{-1})	5.78 × 10^{-2} ± 1.29 × 10^{-2}	8.95 × 10^{-2} ± 1.89 × 10^{-2}	7.64 × 10^{-2} ± 1.00 × 10^{-2}
Microbial loop (mmol C m^{-2} d^{-1})	3.26 ± 0.09	3.17 ± 0.10	2.09 ± 0.05
Xenophyophores			
Uptake (mmol C m^{-2} d^{-1})	0.63 ± 3.12 × 10–2	0.53 ± 3.81 × 10^{-2}	0.32 ± 4.20 × 10^{-2}
Defecation (mmol C m^{-2} d^{-1})	7.31 × 10^{-2} ± 1.52 × 10^{-2}	5.24 × 10^{-2} ± 2.42 × 10^{-2}	8.23 × 10^{-2} ± 1.51 × 10^{-2}
Respiration (mmol C m^{-2} d^{-1})	2.94 × 10^{-3} ± 7.72 × 10^{-3}	2.05 × 10^{-3} ± 6.11 × 10^{-3}	1.73 × 10^{-3} ± 3.07 × 10^{-3}
Respiration rate (d^{-1})	4.03 × 10^{-3}	3.46 × 10^{-3}	6.87 × 10^{-3}
Production rate (d^{-1})	0.75	0.81	0.94
AE (–)	0.88	0.90	0.71
GE (–)	0.995	0.996	0.996

Appendix B. Supplementary material

Supplementary data to this article can be found online at https://doi.org/10.1016/j.pocean.2020.102446.

References

Allesina, S., Pascual, M., 2008. Network structure, predator - Prey modules, and stability in large food webs. Theor. Ecol. 1, 55–64. https://doi.org/10.1007/s12080-007-0007-8.

Amon, D.J., Ziegler, A.F., Dahlgren, T.G., Glover, A.G., Goineau, A., Gooday, A.J., Wiklund, H., Smith, C.R., 2016. Insights into the abundance and diversity of abyssal megafauna in a polymetallic-nodule region in the eastern Clarion-Clipperton Zone. Sci. Rep. 6, 30492. https://doi.org/10.1038/srep30492.

Arifin, Z., Bendell-Young, L.I., 1997. Feeding response and carbon assimilation by the blue mussel *Mytilus trossulus* exposed to environmentally relevant seston matrices. Mar. Ecol. Prog. Ser. 160, 241–253.

Baumgarten, S., Laudien, J., Jantzen, C., Häussermann, V., Försterra, G., 2014. Population structure, growth and production of a recent brachiopod from the Chilean fjord region. Mar. Ecol. 35, 401–413. https://doi.org/10.1111/maec.12097.

Bayne, B.L., Iglesias, J.I.P., Hawkins, A.J.S., Navarro, E., Heral, M., Deslous-Paoli, J.M., 1993. Feeding behaviour of the mussel, *Mytilus edulis*: responses to variations in quantity and organic content of the seston. J. Mar. Biol. Assoc. UK 73, 813–829.

Bharatdwaj, K., 2006. Reliefs of the ocean basins, in: Physical Geography (Oceanography). Discovery Publishing House, New Delhi, pp. 1–53.

Bianchelli, S., Gambi, C., Zeppilli, D., Danovaro, R., 2010. Metazoan meiofauna in deep-sea canyons and adjacent open slopes: A large-scale comparison with focus on the rare taxa. Deep-Sea Res. I 57, 420–433. https://doi.org/10.1016/j.dsr.2009.12.001.

Billett, D.S., Bett, B., Rice, A., Thurston, M., Galéron, J., Sibuet, M., Wolff, G., 2001. Long-term change in the megabenthos of the Porcupine Abyssal Plain (NE Atlantic). Prog. Oceanogr. 50, 325–348. https://doi.org/10.1016/S0079-6611(01)00060-X.

Bluhm, H., 2001. Re-establishment of an abyssal megabenthic community after experimental physical disturbance of the seafloor. Deep-Sea Res. II 48, 3841–3868. https://doi.org/10.1016/S0967-0645(01)00070-4.
Boetius, A., 2015. RV SONNE SO242/2. Cruise Report/Fahrtbericht. DISCOL revisited. Guayaquil: 28 August 2015 - Guayaquil: 1 October 2015. SO242/2: JPI Oceans Ecological Aspects of Deep-Sea Mining. Bremen.
Boetius, A., Lochte, K., 1996. Effect of organic enrichments on hydrolytic potentials and growth of bacteria in deep-sea sediments. Mar. Ecol. Prog. Ser. 140, 239–250. https://doi.org/10.3354/meps140239.
Brey, T., Clarke, A., 1993. Population dynamics of marine benthic invertebrates in Antarctic and subantarctic environments: Are there unique adaptations? Antarct. Sci. 5, 253–266. https://doi.org/10.1017/S0954102093000343.
Brey, T., Gutt, J., Mackensen, A., Starmans, A., 1998. Growth and productivity of the high Antarctic bryozoan *Melicerita obliqua*. Mar. Biol. 132, 327–333. https://doi.org/10.1007/s002270050398.
Brey, T., Hain, S., 1992. Growth, reproduction and production of *Lissarca notorcadensis* (Bivalvia: Philobryidae) in the Weddell Sea. Antarctica. Mar. Ecol. Prog. Ser. 82, 219–226.
Brey, T., Müller-Wiegmann, C., Zittier, Z.M.C., Hagen, W., Marina, S., 2010. Body composition in aquatic organisms - A global data bank of relationships between mass, elemental composition and energy content. J. Sea Res. 64, 334–340. https://doi.org/10.1016/j.seares.2010.05.002.
Brey, T., Peck, L.S., Gutt, J., Hain, S., Arntz, W.E., 1995. Population dynamics of *Magellania fragilis*, a brachiopod dominating a mixed-bottom macrobenthic assemblage on the Antarctic shelf. J. Mar. Biol. Assoc. UK 75, 869–887.
Brown, A., Hauton, C., Stratmann, T., Sweetman, A., van Oevelen, D., Jones, D.O.B., 2018. Metabolic rates are significantly lower in abyssal Holothuroidea than in shallow-water Holothuroidea. R. Soc. Open Sci. 5, 172162 https://doi.org/10.1098/rsos.172162.
Buchanan, J.B., 1984. Sediment analysis. In: Holme, N.A., McIntyre, A.D. (Eds.), Methods for the Study of Marine Benthos. Blackwell Scientific Publications. pp. 41–65.
Burkepile, D.E., Parker, J.D., Woodson, C.B., Mills, H.J., Kubanek, J., Sobecky, P.A., Hay, M.E., 2006. Chemically mediated competition between microbes and animals: Microbes as consumers in food webs. Ecology 87, 2821–2831. https://doi.org/10.1890/0012-9658(2006)87[2821:CMCBMA]2.0.CO;2.
Camacho, A.P., Labarta, U., Navarro, E., 2000. Energy balance of mussels *Mytilus galloprovincialis*: the effect of length and age. Mar. Ecol. Prog. Ser. 199, 149–158.
Cammen, L.M., Seneca, E.D., Stroud, L.M., 1980. Energy flow through the fiddler crabs *Uca pugnax* and *U. minax* and the marsh periwinkle *Littorina irrorata* in a North Carolina salt marsh. Am. Midl. Nat. 103, 238. https://doi.org/10.2307/2424622.
Cartes, J.E., Elizalde, M., Sorbe, J.C., 2001. Contrasting life-histories, secondary production, and trophic structure of Peracarid assemblages of the bathyal suprabenthos from the Bay of Biscay (NE Atlantic) and the Catalan Sea (NW Mediterranean). Deep-Sea Res. I 48, 2209–2232. https://doi.org/10.1016/S0967-0637(01)00012-7.
Cartes, J.E., Mamouridis, V., Fanelli, E., 2011. Deep-sea suprabenthos assemblages (Crustacea) off the Balearic Islands (western Mediterranean): Mesoscale variability in diversity and production. J. Sea Res. 65, 340–354. https://doi.org/10.1016/j.seares.2011.02.002.
Cartes, J.E., Sorbe, J.C., 1999. Estimating secondary production in bathyal suprabenthic peracarid crustaceans from the Catalan Sea slope (western Mediterranean; 391–1255 m). J. Exp. Mar. Bio. Ecol. 239, 195–210. https://doi.org/10.1016/S0022-0981(99)00026-X.
Ceccherelli, V.U., Mistri, M., 1991. Production of the meiobenthic harpacticoid copepod *Canuella perplexa*. Mar. Ecol. Prog. Ser. 68, 225–234.
Childress, J.J., Taylor, S.M., Cailliet, G.M., Price, M.H., Cailliert, G.M., Price, M.H., 1980. Patterns of growth, energy utilization and reproduction in some meso-and bathypelagic fishes off Southern California. Mar. Biol. 61, 27–40. https://doi.org/10.1007/BF00410339.
Cho, H., Kim, K.H., Son, S.K., Hyun, J.H., 2018. Fine-scale microbial communities associated with manganese nodules in deep-sea sediment of the Korea deep ocean study area in the Northeast Equatorial Pacific. Ocean Sci. J. 53, 337–353. https://doi.org/10.1007/s12601-018-0032-0.
Christensen, V., Pauly, D., 1992. Ecopath II – a software for balancing steady-state ecosystem models and calculating network characteristics. Ecol. Modell. 61, 169–185.
Clausen, I., Riisgård, H.U.H., 1996. Growth, filtration and respiration in the mussel *Mytilus edulis*: no evidence for physiological regulation of the filter-pump to nutritional needs. Mar. Ecol. Prog. Ser. 141, 37–45. https://doi.org/10.3354/meps141037.
Collins, M.A., Bailey, D.D.M., Ruxton, G.D., Priede, I.I.G., 2005. Trends in body size across an environmental gradient: A differential response in scavenging and non-scavenging demersal deep-sea fish. Proc. R. Soc. B Biol. Sci. 272, 2051–2057. https://doi.org/10.1098/rspb.2005.3189.
Connor, K.M., Sung, A., Garcia, N.S., Gracey, A.Y., German, D.P., 2016. Modulation of digestive physiology and biochemistry in *Mytilus californianus* in response to feeding level acclimation and microhabitat. Biol. Open 5, 1200–1210. https://doi.org/10.1242/bio.019430.
Cox, T.E., Murray, S.N., 2006. Feeding preferences and the relationships between food choice and assimilation efficiency in the herbivorous marine snail *Lithopoma undosum* (Turbinidae). Mar. Biol. 148, 1295–1306. https://doi.org/10.1007/s00227-005-0166-3.
Crabtree, R.E., Carter, J., Musick, J.A., 1991. The comparative feeding ecology of temperate and tropical deep- sea fishes from the western North Atlantic. Deep-Sea Res. 38, 1277–1298.
Crisp, D., 1971. Energy flow measurements. In: Holme, N.A., McIntyre, A.D. (Eds.), Methods for the Study of Marine Benthos. Blackwell Scientific Publications, pp. 284–367.
Danovaro, R., 2010. Benthic prokaryotic heterotrophic production using the leucin incorporation method. In: Methods for the Study of Deep-Sea Sediments, Their Functioning and Biodiversity. CRC Press – Taylor & Francis Group, Boca Raton, pp. 337–342.
Danovaro, R., Dell'Anno, A., Corinaldesi, C., Magagnini, M., Noble, R., Tamburini, C., Weinbauer, M., 2008. Major viral impact on the functioning of benthic deep-sea ecosystems. Nature 454, 1084–1087. https://doi.org/10.1038/nature07268.
De Jonge, V.N., 1980. Fluctuations in the organic carbon to chlorophyll a ratios for estuarine benthic diatom populations. Mar. Ecol. Prog. Ser. 2, 345–353. https://doi.org/10.3354/meps002345.
De Smet, B., Pape, E., Riehl, T., Bonifácio, P., Colson, L., Vanreusel, A., 2017. The community structure of deep-sea macrofauna associated with polymetallic nodules in the eastern part of the Clarion-Clipperton Fracture Zone. Front. Mar. Sci. 4, 14. https://doi.org/10.3389/fmars.2017.00103 Deep-sea.
DeLaca, T.E., Karl, D.M., Lipps, J.H., 1981. Direct use of dissolved organic carbon by agglutinated benthic Foraminifera. Nature 289, 287–289.
Deming, J.W., 1985. Bacterial growth in deep-sea sediment trap and boxcore samples. Mar. Ecol. Prog. Ser. 25, 305–312. https://doi.org/10.3354/meps025305.
Drazen, J.C., Leitner, A., Morningstar, S., Marcon, Y., Greinert, J., Purser, A., 2019. Observations of deep-sea fishes and mobile scavengers from the abyssal DISCOL experimental mining area. Biogeosciences 16, 3133–3146. https://doi.org/10.5194/bg-16-3133-2019.
Drazen, J.C., Reisenbichler, K.R., Robison, B.H., 2007. A comparison of absorption and assimilation efficiencies between four species of shallow- and deep-living fishes. Mar. Biol. 151, 1551–1558. https://doi.org/10.1007/s00227-006-0596-6.
Drazen, J.C., Seibel, B.A., 2007. Depth-related trends in metabolism of benthic and benthopelagic deep-sea fishes. Limnol. Oceanogr. 52, 2306–2316. https://doi.org/10.4319/lo.2007.52.5.2306.
Drazen, J.C., Smith, C.R., Gjerde, K.M., Haddock, S.H.D., Carter, G.S., Choy, C.A., Clark, M.R., Dutrieux, P., Goetze, E., Hauton, C., Hatta, M., Koslow, J.A., Leitner, A.B., Pacini, A., Perelman, J.N., Peacock, T., Sutton, T.T., Watling, L., Yamamoto, H., 2020. Opinion: Midwater ecosystems must be considered when evaluating environmental risks of deep-sea mining. PNAS 117, 17455–17460. https://doi.org/10.1073/pnas.2011914117.
Drazen, J.C., Sutton, T.T., 2017. Dining in the deep: The feeding ecology of deep-sea fishes. Ann. Rev. Mar. Sci. 9, 337–366. https://doi.org/10.1146/annurev-marine-010816-060543.
Drazen, J.C., Yeh, J., 2012. Respiration of four species of deep-sea demersal fishes measured in situ in the eastern North Pacific. Deep-Sea Res. I 60, 1–6. https://doi.org/10.1016/j.dsr.2011.09.007.
Dunlop, K.M., van Oevelen, D., Ruhl, H.A., Huffard, C.L., Kuhnz, L.A., Smith, K.L., 2016. Carbon cycling in the deep eastern North Pacific benthic food web: Investigating the effect of organic carbon input. Limnol. Oceanogr. 61, 1956–1968. https://doi.org/10.1002/lno.10345.
Durden, J.M., Ruhl, H.A., Pebody, C., Blackbird, S.J., van Oevelen, D., 2017. Differences in the carbon flows in the benthic food webs of abyssal hill and plain habitats. Limnol. Oceanogr. 62, 1771–1782. https://doi.org/10.1002/lno.10532.
Durden, J.M., Bett, B.J., Horton, T., Serpell-Stevens, A., Morris, K.J., Billett, D.S.M., Ruhl, H.A., 2016. Improving the estimation of deep-sea megabenthos biomass: Dimension to wet weight conversions for abyssal invertebrates. Mar. Ecol. Prog. Ser. 552, 71–79. https://doi.org/10.3354/meps11769.
Enríquez-García, C., Nandini, S., Sarma, S.S.S., 2013. Feeding behaviour of *Acanthocyclops americanus* (Marsh) (Copepoda: Cyclopoida). J. Nat. Hist. 47, 853–862. https://doi.org/10.1080/00222933.2012.747637.
Enríquez-Ocaña, L.F., Nieves-Soto, M., Piña-Valdez, P., Martinez-Cordova, L.R., Medina-Jasso, M.A., 2012. Evaluation of the combined effect of temperature and salinity on the filtration, clearance rate and assimilation efficiency of the mangrove oyster *Crassostrea corteziensis* (Hertlein, 1951). Arch. Biol. Sci. 64, 479–488. https://doi.org/10.2298/ABS1202479O.
Escobar-Briones, E., Morales, P., Cienfuegos, E., González, M., 2002. Carbon sources and trophic position of two abyssal species of Anomura, *Munidopsis alvisca* (Galatheidae) and *Neolithodes diomedeae* (Lithodidae). Contrib. to Study East Pacific Crustac. 1, 37–43.
Fabiano, M., Danovaro, R., Fraschetti, S., 1995. A three-year time series of elemental and biochemical composition of organic matter in subtidal sandy sediments of the Ligurian Sea (northwestern Mediterranean). Cont. Shelf Res. 15, 1453–1469. https://doi.org/10.1016/0278-4343(94)00088-5.
Finn, J.T., 1976. Measures of ecosystem structure and function derived from analysis of flows. J. Theor. Biol. 56, 363–380. https://doi.org/10.1016/S0022-5193(76)80080-X.
Fleeger, J.W., Palmer, M.A., 1982. Secondary production of the estuarine, meiobenthic copepod *Microarthridion littorale*. Mar. Ecol. Prog. Ser. 7, 157–162. https://doi.org/10.3354/meps007157.
Fox, R., Barnes, R.D., Ruppert, E., 2003. Invertebrate Zoology: A Functional Evolutionary Approach, 7 ed. Brooks/Cole Thompson Learning, Belmont, California.
Fratt, D.B., Dearborn, J.H., 1984. Feeding biology of the Antarctic brittle star *Ophionotus victoriae* (Echinodermata: Ophiuroidea). Polar Biol. 3, 127–139. https://doi.org/10.1007/BF00442644.
Froese, R., Thorson, J.T., Reyes, R.B., 2014. A Bayesian approach for estimating length-weight relationships in fishes. J. Appl. Ichthyol. 30, 78–85. https://doi.org/10.1111/jai.12299.

Fukuda, R., Ogawa, H., Nagata, T., Koike, I., 1998. Direct determination of carbon and nitrogen contents of natural bacterial assemblages in marine environments. Appl. Environ. Microbiol. 64, 3352–3358.
Gage, J.D., Tyler, P.A., 1991. Deep-sea Biology: A Natural History of Organisms at the Deep-Sea Floor. Cambridge University Press, Cambridge, UK.
Galéron, J., Sibuet, M., Mahaut, M., Dinet, A., 2000. Variation in structure and biomass of the benthic communities at three contrasting sites in the tropical Northeast Atlantic. Mar. Ecol. Prog. Ser. 197, 121–137. https://doi.org/10.3354/meps197121.
Gardner, M.R., Ashby, W.R., 1970. Connectance of large dynamic (Cybernetic) systems: Critical values for stability. Nature 228, 784. https://doi.org/10.1038/228784a0.
Gausepohl, F., Hennke, A., Schoening, T., Köser, K., Greinert, J., 2020. Scars in the abyss: reconstructing sequence, location and temporal change of the 78 plough tracks of the 1989 DISCOL deep-sea disturbance experiment in the Peru Basin. Biogeosciences 17, 1463–1493. https://doi.org/10.5194/bg-17-1463-2020.
Gerlach, S.A., Hahn, A.E., Schrage, M., 1985. Size spectra of benthic biomass and metabolism. Mar. Ecol. Prog. Ser. 26, 161–173.
Gerringer, M.E., Popp, B.N., Linley, T.D., Jamieson, A.J., Drazen, J.C., 2017. Comparative feeding ecology of abyssal and hadal fishes through stomach content and amino acid isotope analysis. Deep-Sea Res. I 121, 110–120. https://doi.org/10.1016/j.dsr.2017.01.003.
Geslin, E., Risgaard-Petersen, N., Lombard, F., Metzger, E., Langlet, D., Jorissen, F., 2011. Oxygen respiration rates of benthic foraminifera as measured with oxygen microsensors. J. Exp. Mar. Bio. Ecol. 396, 108–114.
Giere, O., 2009. Meiobenthology. The microscopic motile fauna of aquatic sediments, 2 ed. Springer-Verlag, Berlin.
Giere, O., 2006. Ecology and biology of marine Oligochaeta – an inventory rather than another review. Hydrobiologia 564, 103–116. https://doi.org/10.1007/s10750-005-1712-1.
Gollner, S., Kaiser, S., Menzel, L., Jones, D.O.B., Brown, A., Mestre, N.C., van Oevelen, D., Menot, L., Colaço, A., Canals, M., Cuvelier, D., Durden, J.M., Gebruk, A., Egho, G.A., Haeckel, M., Marcon, Y., Mevenkamp, L., Morato, T., Pham, C.K., Purser, A., Sanchez-Vidal, A., Vanreusel, A., Vink, A., Martinez Arbizu, P., 2017. Resilience of benthic deep-sea fauna to mining activities. Mar. Environ. Res. 129, 76–101. https://doi.org/10.1016/j.marenvres.2017.04.010.
Gooday, A.J., Bett, B.J., Pratt, D.N., 1993. Direct observation of episodic growth in an abyssal xenophyophore (Protista). Deep. Res. I 40, 2131–2143. https://doi.org/10.1016/0967-0637(93)90094-J.
Gooday, A.J., Carstens, M., Thiel, H., 1995. Micro- and Nanoforaminifera from abyssal Northeast Atlantic sediments: A preliminary report. Int. Rev. ges. Hydrobiol. Hydrogr. 80, 361–383. https://doi.org/10.1002/iroh.19950800223.
Gooday, A.J., Levin, L.A., Linke, P., Heeger, T., 1992. The role of benthic foraminifera in deep-sea food webs and carbon cycling. Deep-Sea Food Chains and the Global Carbon Cycle. Kluwer Academic Publisher, Dordrecht, pp. 63–91.
Gooday, A.J., Schoenle, A., Dolan, J.R., Arndt, H., 2020. Protist diversity and function in the dark ocean – Challenging the paradigms of deep-sea ecology with special emphasis on foraminiferans and naked protists. Eur. J. Protistol. 75, 125721. https://doi.org/10.1016/j.ejop.2020.125721.
Gooday, A.J., Sykes, D., Góral, T., Zubkov, M.V., Glover, A.G., 2018. Micro-CT 3D imaging reveals the internal structure of three abyssal xenophyophore species (Protista, Foraminifera) from the eastern equatorial Pacific Ocean. Sci. Rep. 8, 1–12.
Gorny, M., Brey, T., Arntz, W.E., Bruns, T., 1993. Growth, development and productivity of *Chorismus antarcticus* (Pfeffer) (Crustacea: Decapoda: Natantia) in the eastern Weddell Sea, Antarctica. J. Mar. Biol. Assoc. UK 174, 261–275.
Gowing, M.M., Wishner, K.F., 1986. Trophic relationships of deep-sea calanoid copepods from the benthic boundary layer of the Santa Catalina Basin, California. Deep-Sea Res. 33, 939–962.
Grahame, J., 1973. Assimilation efficiency of *Littorina littorea* (L.) (Gastropoda: Prosobranchiata). J. Anim. Ecol. 42, 383–389.
Greinert, J., 2015. RV SONNE Fahrtbericht/Cruise Report SO242-1 – JPI OCEANS Ecological Aspects of Deep-Sea Mining – DISCOL Revisited.
Griffiths, R.J., 1980. Filtration, repiration and assimilation in the Black Mussel *Choromytilus meridionalis*. Mar. Ecol. Prog. Ser. 3, 63–70. https://doi.org/10.3354/meps003063.
Haeckel, M., Konig, I., Riech, V., Weber, M.E.M.E., Suess, E., König, I., Riech, V., Weber, M.E., Suess, E., 2001. Pore water profiles and numerical modelling of biogeochemical processes in Peru Basin deep-sea sediments. Deep-Sea Res. II 48, 3713–3736.
Haffert, L., Haeckel, M., de Stigter, H., Janssen, F., 2020. Assessing the temporal scale of deep-sea mining impacts on sediment biogeochemistry. Biogeosciences 17, 2767–2789. https://doi.org/10.5194/bg-17-2767-2020.
Han, K.N., Lee, S.W., Wang, S.Y., 2008. The effect of temperature on the energy budget of the Manila clam, *Ruditapes philippinarum*. Aquac. Int. 16, 143–152. https://doi.org/10.1007/s10499-007-9133-y.
Harbour, R.P., Leitner, A.B., Ruehlemann, C., Vink, A., Sweetman, A.K., 2020. Benthic and demersal scavenger biodiversity in the eastern end of the Clarion-Clipperton Zone – an area marked for polymetallic nodule mining. Front. Mar. Sci. 7, 458. https://doi.org/10.3389/fmars.2020.00458.
Hein, J.R., Mizell, K., Koschinsky, A., Conrad, T.A., 2013. Deep-ocean mineral deposits as a source of critical metals for high- and green-technology applications: Comparison with land-based resources. Ore Geol. Rev. 51, 1–14. 10.1016/j.oregeorev.2012.12.001.
Heiner, I., Vinther Sørensen, M., Møbjerg Kristensen, R., 2018. Loricifera (Girdle Wearers). Grzimek's Anim, Life Encycl.
Herman, P.M.J., Vranken, G., 1988. Studies of the life-history and energetics of marine and brackish-water nematodes. Oecologia 77, 457–463.
Heymans, J.J., Coll, M., Libralato, S., Morissette, L., Christensen, V., 2014. Global patterns in ecological indicators of marine food webs: A modelling approach. PLoS One 9. https://doi.org/10.1371/journal.pone.0095845.
Higgins, R.P., Thiel, H., 1988. Introduction to the Study of Meiofauna. Smithsonian Institution Press.
Hoshino, T., Inagaki, F., 2019. Abundance and distribution of Archaea in the subseafloor sedimentary biosphere. ISME Journal 13, 227–231. https://doi.org/10.1038/s41396-018-0253-3.
Hudson, I.R., Pond, D.W., Billett, D.S.M., Tyler, P.A., Lampitt, R.S., Wolff, G.A., 2004. Temporal variations in fatty acid composition of deep-sea holothurians: Evidence of bentho-pelagic coupling. Mar. Ecol. Prog. Ser. 281, 109–120. https://doi.org/10.3354/meps281109.
Hughes, J.A., Gooday, A.J., 2004. Associations between living benthic foraminifera and dead tests of *Syringammina fragilissima* (Xenophyophorea) in the Darwin Mounds region (NE Atlantic). Deep-Sea Res. I 51, 1741–1758. https://doi.org/10.1016/j.dsr.2004.06.004.
Hughes, R.N., 1971. Ecological energetics of *Nerita* (Archaeogastropoda, Neritacea) populations on Barbados, West Indies. Mar. Biol. 11, 12–22. https://doi.org/10.1007/BF00348016.
Hughes, S.J.M., 2010. Towards deep-sea toxicology: Experimental approaches with echinoderms. University of Southampton, Southampton. PhD-Thesis.
Hughes, S.J.M., Ruhl, H.A., Hawkins, L.E., Hauton, C., Boorman, B., Billett, D.S.M., 2011. Deep-sea echinoderm oxygen consumption rates and an interclass comparison of metabolic rates in Asteroidea, Crinoidea, Echinoidea, Holothuroidea and Ophiuroidea. J. Exp. Biol. 214, 2512–2521. https://doi.org/10.1242/jeb.055954.
Hunt, H.W., Coleman, D.C., Ingham, E.R., Ingham, R.E., Elliott, E.T., Moore, J.C., Rose, S.L., Reid, C.P.P., Morley, C.R.I., 1987. The detrital food web in a shortgrass prairie. Biol 3, 57–68.
Ibarrola, I., Iglesias, J.I.P., Urrutia, M.B., 2000. Temporal changes of feeding and absorption of biochemical components in *Cerastoderma edule* fed an algal diet. J. Mar. Biol. Assoc. UK 80, 119–125.
Iken, K., Brey, T., Wand, U., Voigt, J., Junghans, P., 2001. Food web structure of the benthic community at the Porcupine Abyssal Plain (NE Atlantic): A stable isotope analysis. Prog. Oceanogr. 50, 383–405. https://doi.org/10.1016/S0079-6611(01)00062-3.
Ingole, B.S., Ansari, Z.A., Rathod, V., Rodrigues, N., 2001. Response of deep-sea macrobenthos to a small-scale environmental disturbance. Deep-Sea Res. II 48, 3401–3410. https://doi.org/10.1016/S0967-0645(01)00048-0.
Ingole, B.S., Goltekar, R., Gonsalves, S., Ansari, Z.A., 2005. Recovery of deep-sea meiofauna after artificial disturbance in the Central Indian Basin. Mar. Georesour. Geotechnol. 23, 253–266. https://doi.org/10.1080/10641190500446540.
Ingole, B.S., Pavithran, S., Ansari, Z.A., 2005. Restoration of deep-sea macrofauna after simulated benthic disturbance in the Central Indian Basin. Mar. Georesour. Geotechnol. 23, 267–288. https://doi.org/10.1080/10641190500446573.
Janssen, A., Kaiser, S., Meißner, K., Brenke, N., Menot, L., Martínez Arbizu, P., 2015. A reverse taxonomic approach to assess macrofaunal distribution patterns in abyssal Pacific polymetallic nodule fields. PLoS One 10, e0117790. https://doi.org/10.1371/journal.pone.0117790.
Jeffrey, S.W., Humphrey, G.F., 1975. New spectrophotometric equations for determining chlorophylls a, b, c_1 and c_2 in higher plants, algae and natural phytoplankton. Biochem. und Physiol. der Pflanz. 167, 191–194. https://doi.org/10.1016/S0015-3796(17)30778-3.
Johnson, W.S., 1976. Population energetics of the intertidal isopod *Cirolana harfordi*. Mar. Biol. 36, 351–357. https://doi.org/10.1007/BF00389197.
Jones, D.O.B., Kaiser, S., Sweetman, A.K., Smith, C.R., Menot, L., Vink, A., Trueblood, D., Greinert, J., Billett, D.S.M., Arbizu, P.M., Radziejewska, T., Singh, R., Ingole, B., Stratmann, T., Simon-Lledó, E., Durden, J.M., Clark, M.R., 2017. Biological responses to disturbance from simulated deep-sea polymetallic nodule mining. PLoS One 12. https://doi.org/10.1371/journal.pone.0171750.
Jordana, E., Charles, F., Grémare, A., Amouroux, J.-M., Chrétiennot-Dinet, M.-J., 2001. Food sources, ingestion and absorption in the suspension-feeding polychaete, *Ditrupa arietina* (O. F. Müller). J. Exp. Mar. Bio. Ecol. 266, 219–236. https://doi.org/10.1016/S0022-0981(01)00357-4.
Jørgensen, B.B., Boetius, A., 2007. Feast and famine - Microbial life in the deep-sea bed. Nat. Rev. Microbiol. 5, 770–781. https://doi.org/10.1038/nrmicro1745.
Jumars, P.A., Dorgan, K.M., Lindsay, S.M., 2015. Diet of worms emended: an update of polychaete feeding guilds. Ann. Rev. Mar. Sci. 7, 497–520. https://doi.org/10.1146/annurev-marine-010814-020007.
Khripounoff, A., Caprais, J.C., Decker, C., Le Bruchec, J., Noel, P., Husson, B., 2017. Respiration of bivalves from three different deep-sea areas: Cold seeps, hydrothermal vents and organic carbon-rich sediments. Deep-Sea Res. II 142, 233–243. https://doi.org/10.1016/j.dsr2.2016.05.023.
Klein, H., 1993. Near-bottom currents in the deep Peru Basin. DISCOL experimental area. Dtsch. Hydrogr. Zeitschrift 45, 31–42. https://doi.org/10.1007/BF02226550.
Kones, J.K., Soetaert, K., van Oevelen, D., Owino, J.O., 2009. Are network indices robust indicators of food web functioning? A Monte Carlo approach. Ecol. Modell. 220, 370–382. https://doi.org/10.1016/j.ecolmodel.2008.10.012.
Koopmans, M., Martens, D., Wijffels, R.H., 2010. Growth efficiency and carbon balance for the sponge *Haliclona oculata*. Mar. Biotechnol. 12, 340–349. https://doi.org/10.1007/s10126-009-9228-8.
Korsun, S., Hald, M., Panteleeva, N., Tarasov, G., Båmstedt, U., 1998. Biomass of foraminifera in the St. Anna Trough, Russian Arctic continental margin. Sarsia 83, 419–431.
Koschinsky, A., Borowski, C., Halbach, P., 2003. Reactions of the heavy metal cycle to industrial activities influence on heavy metal cycle in the deep sea. Int. Rev. Hydrobiol. 88, 102–127.

Kreeger, D.A., Newell, R.I.E., 2001. Seasonal utilization of different seston carbon sources by the ribbed mussel, *Geukensia demissa* (Dillwyn) in a mid-Atlantic salt marsh. J. Exp. Mar. Bio. Ecol. 260, 71–91. https://doi.org/10.1016/S0022-0981(01)00242-8.

Labarta, U., Fernández-Reiríz, M.J., Babarro, J.M.F., 1997. Differences in physiological energetics between intertidal and raft cultivated mussels *Mytilus galloprovincialis*. Mar. Ecol. Prog. Ser. 152, 167–173. https://doi.org/10.3354/meps152167.

Lahajnar, N., Rixen, T., Schäfer, P., Ittekkot, V., 2005. Dissolved organic carbon (DOC) fluxes of deep-sea sediments from the Arabian Sea and NE Atlantic. Deep-Sea Res. II 52, 1947–1964. https://doi.org/10.1016/J.DSR2.2005.05.006.

Latham, L.G., 2006. Network flow analysis algorithms. Ecol. Modell. 192, 586–600. https://doi.org/10.1016/j.ecolmodel.2005.07.029.

Laubier, L., Monniot, C., 1985. Peuplements profonds du Golfe de Gascogne. Campagnes BIOGAS, Ifremer, Paris.

Laureillard, J., Méjanelle, L., Sibuet, M., 2004. Use of lipids to study the trophic ecology of deep-sea xenophyophores. Mar. Ecol. Prog. Ser. 270, 129–140. https://doi.org/10.3354/meps270129.

Lee, S.Y., 1997. Potential trophic importance of the faecal material of the mangrove sesarmine crab *Sesarma messa*. Mar. Ecol. Prog. Ser. 159, 275–284. https://doi.org/10.3354/meps159275.

Levin, L.A., 1991. Interactions between metazoans and large, agglutinating protozoans: Implications for the community structure of deep-sea benthos. Integr. Comp. Biol. 31, 886–900. https://doi.org/10.1093/icb/31.6.886.

Levin, L.A., Gooday, A.J., 1992. Possible roles for xenophyophores in deep-sea carbon cycling. Deep Food Chain Glob. Carbon Cycle 93–104. https://doi.org/10.1007/978-94-011-2452-2_6.

Lindh, M.V., Maillot, B.M., Shulse, C.N., Gooday, A.J., Amon, D.J., Smith, C.R., Church, M.J., 2017. From the surface to the deep-sea: Bacterial distributions across polymetallic nodule fields in the Clarion-Clipperton Zone of the Pacific Ocean. Front. Microbiol. 8, 1–12. https://doi.org/10.3389/fmicb.2017.01696.

Linley, T.D., 2014. Atlas of Abyssal Megafauna Morphotypes of the Clipperton-Clarion Fracture Zone: Osteichthyes [WWW Document]. Online Identif, Guid.

Lochte, K., Turley, C.M., 1988. Bacteria and cyanobacteria associated with phytodetritus in the deep sea. Nature 333, 67–69. https://doi.org/10.1038/333067a0.

Luna, G.M., Corinaldesi, C., Rastelli, E., Danovaro, R., 2013. Patterns and drivers of bacterial α- and β-diversity across vertical profiles from surface to subsurface sediments. Environ. Microbiol. Rep. 5, 731–739. https://doi.org/10.1111/1758-2229.12075.

MacAvoy, S.E., Carney, R.S., Morgan, E., Macko, S.A., 2008. Stable isotope variation among the mussel *Bathymodiolus childressi* and associated heterotrophic fauna at four cold-seep communities in the Gulf of Mexico. J. Shellfish Res. 27, 147–151. https://doi.org/10.2983/0730-8000(2008)27[147:SIVATM]2.0.CO;2.

Maier, S.R., Kutti, T., Bannister, R.J., van Breugel, P., van Rijswijk, P., van Oevelen, D., 2019. Survival under conditions of variable food availability: Resource utilization and storage in the cold-water coral *Lophelia pertusa*. Limnol. Oceanogr. 64, 1651–1671. https://doi.org/10.1002/lno.11142.

Marcon, Y., Purser, A., 2017. PAPARA(ZZ)I: An open-source software interface for annotating photographs of the deep-sea. SoftwareX 6, 69–80.

McClain, C.R., Johnson, N.A., Rex, M.A., 2004. Morphological disparity as a biodiversity metric in lower bathyal and abyssal gastropod assemblages. Evolution 58, 338–348.

Menzies, R.J.R.J., 1962. On the food and feeding habits of abyssal organisms as exemplified by the Isopoda. Int. Rev. Hydrobiol. 47, 339–358. https://doi.org/10.1002/iroh.19620470303.

Middelburg, J.J., 2019. Marine Carbon Biogeochemistry: A Primer for Earth System Scientists. In: Springer Briefs in Earth System Sciences. https://doi.org/10.1007/978-3-030-10822-9.

Middelburg, J.J., 2018. Reviews and syntheses: To the bottom of carbon processing at the seafloor. Biogeosciences 15, 413–427. https://doi.org/10.5194/bg-15-413-2018.

Middelburg, J.J., 2011. Chemoautotrophy in the ocean. Geophys. Res. Lett. 38, 94–97. https://doi.org/10.1029/2011GL049725.

Miljutin, D.M., Miljutina, M.A., Arbizu, P.M., Galéron, J., 2011. Deep-sea nematode assemblage has not recovered 26 years after experimental mining of polymetallic nodules (Clarion-Clipperton Fracture Zone, Tropical Eastern Pacific). Deep-Sea Res. I 58, 885–897. https://doi.org/10.1016/j.dsr.2011.06.003.

Miller, K.A., Thompson, K.F., Johnston, P., Santillo, D., 2018. An overview of seabed mining including the current state of development, environmental impacts, and knowledge gaps. Front. Mar. Sci. 4, 418. https://doi.org/10.3389/fmars.2017.00418.

Miller, R.J., Smith, C.R., Demaster, D.J., Fornes, W.L., 2000. Feeding selectivity and rapid particle processing by deep-sea megafaunal deposit feeders: A ^{234}Th tracer approach. J. Mar. Res. 58, 653–673. https://doi.org/10.1357/002224000321511061.

Mistri, M., Rossi, R., Fano, E.A.A., 2001. Structure and secondary production of a soft bottom macrobenthic community in a brackish lagoon (Sacca di Goro, north-eastern Italy). Estuar. Coast. Mar. Sci. 52, 605–616. https://doi.org/10.1006/ecss.2001.0757.

Mojtahid, M., Zubkov, M.V., Hartmann, M., Gooday, A.J., 2011. Grazing of intertidal benthic foraminifera on bacteria: Assessment using pulse-chase radiotracing. J. Exp. Mar. Bio. Ecol. 399, 25–34.

Molari, M., Janssen, F., Vonnahme, T.R., Wenzhöfer, F., Boetius, A., 2020. The contribution of microbial communities in polymetallic nodules to the diversity of the deep-sea microbiome of the Peru Basin (4130–4198m depth). Biogeosciences 17, 3203–3222. https://doi.org/10.5194/bg-17-3203-2020.

Molari, M., Manini, E., Dell'Anno, A., 2013. Dark inorganic carbon fixation sustains the functioning of benthic deep-sea ecosystems. Global Biogeochem. Cycles 27, 212–221. https://doi.org/10.1002/gbc.20030.

Mondal, S., 2006. Effect of temperature and body size on food utilization in the marine pearl oyster *Pinctada fucata* (Bivalvia: Pteridae). Indian J. Mar. Sci. 35, 43–49.

Murphy, K., Goulding, L., Munro, C., Ward, J., Martin, A., 2016. Register of main impacts and causative factors. MIDAS deliverable 7.3. London.

Nakamura, M., Chen, C., Mitarai, S., 2015. Insights into life-history traits of *Munidopsis* spp. (Anomura: Munidopsidae) from hydrothermal vent fields in the Okinawa Trough, in comparison with the existing data. Deep-Sea Res. I 100, 48–53. https://doi.org/10.1016/J.DSR.2015.02.007.

Navarro, E., Iglesias, J.I.P., Ortega, M.M., 1992. Natural sediment as a food source for the cockle *Cerastoderma edule* (L.): effect of variable particle concentration on feeding, digestion and the scope for growth. J. Exp. Biol. 156, 69–87.

Navarro, E., Iglesias, J.I.P., Ortega, M.M., Larretxea, X., 1994. The basis for a functional response to variable food quantity and quality in cockles *Cerastoderma edule* (Bivalvia, Cardiidae). Physiol. Zool. 67, 468–496.

Navarro, J.M., Thompson, R.J., 1996. Physiological energetics of the horse mussel *Modiolus modiolus* in a cold ocean environment. Mar. Ecol. Prog. Ser. 138, 135–148. https://doi.org/10.3354/meps138135.

Nelson, E.J., MacDonald, B.A., Robinson, S.M.C., 2012. The absorption efficiency of the suspension-feeding sea cucumber, *Cucumaria frondosa*, and its potential as an extractive integrated multi-trophic aquaculture (IMTA) species. Aquaculture 370–371, 19–25. https://doi.org/10.1016/j.aquaculture.2012.09.029.

Nielsen, A.M., Eriksen, N.T., Lønsmann Iversen, J.J., Riisgård, H.U., 1995. Feeding, growth and respiration in the polychaetes *Nereis diversicolor* (facultative filter-feeder) and *N. virens* (omnivorous) – a comparative study. Mar. Ecol. Prog. Ser. 125, 149–158. https://doi.org/10.3354/meps125149.

Nieves-Soto, M., Fernando-Bucle Ramirez, L., Piña-Valdez, P., Medina-Jasso, M.A., Miranda-Baeza, A., Martínez-Córdova, L.R., López-Elías, J.A., 2013. Combined effect of temperature and food concentration on the filtration and clarification rates and assimilation efficiency of *Atrina tuberculosa* Sowerby, 1835 (Mollusca: Bivalvia) under laboratory conditions. Arch. Biol. Sci. 65, 99–106. https://doi.org/10.2298/ABS1301099N.

Niu, C.-J.J., Nakao, S., Goshima, S., 1998. Energetics of the limpet *Lottia kogamogai* (Gastropoda: Acmaeidae) in an intertidal rocky shore in southern Hokkaido, Japan. J. Exp. Mar. Bio. Ecol. 224, 167–181. https://doi.org/10.1016/S0022-0981(97)00190-1.

Nomaki, H., Ogawa, N.O., Takano, Y., Suga, H., Ohkouchi, N., Kitazato, H., 2011. Differing utilization of glucose and algal particulate organic matter by deep-sea benthic organisms of Sagami Bay, Japan. Mar. Ecol. Prog. Ser. 431, 11–24.

Nomaki, H., Yamaoka, A., Shirayama, Y., Kitazato, H., 2007. Deep-sea benthic foraminiferal respiration rates measured under laboratory conditions. J. Foraminifer. Res. 37, 281–286.

Nordhaus, I., Wolff, M., 2007. Feeding ecology of the mangrove crab *Ucides cordatus* (Ocypodidae): Food choice, food quality and assimilation efficiency. Mar. Biol. 151, 1665–1681. https://doi.org/10.1007/s00227-006-0597-5.

Nunnally, C.C., Friedman, J.R., Drazen, J.C., 2016. *In situ* respiration measurements of megafauna in the Kermadec Trench. Deep-Sea Res. I 118, 30–36. https://doi.org/10.1016/j.dsr.2016.10.009.

Oebius, H.U., Becker, H.J., Rolinski, S., Jankowski, J.A., 2001. Parametrization and evaluation of marine environmental impacts produced by deep-sea manganese nodule mining. Deep-Sea Res. II 48, 3453–3467. https://doi.org/10.1016/S0967-0645(01)00052-2.

Orcutt, B.N., Bradley, J., Brazelton, W.J., Estes, E.J., Goordial, J.M., Huber, J.A., Jones, R.M., Mahmoudi, N., Marlow, J.J., Murdock, S., Pachiadaki, M., 2020. Impacts of deep-sea mining on microbial ecosystem services. Limnol. Oceanogr. 65, 1489–1510. https://doi.org/10.1002/lno.11403.

Paul, S.A.L., Gaye, B., Haeckel, M., Kasten, S., Koschinsky, A., 2018. Biogeochemical regeneration of a nodule mining disturbance site: Trace metals, DOC and amino acids in deep-sea sediments and pore waters. Front. Mar. Sci. 5, 117. https://doi.org/10.3389/FMARS.2018.00117.

Peña-Messina, E., Martínez-Córdova, L.R., Bückle-Ramírez, L.F., Segovia-Quintero, M.A., Zertuche-González, J.A., 2009. A preliminary evaluation of physiological filtration variables for *Crassostrea corteziensis* (Hertlein, 1951) and *Anadara tuberculosa* (Sowerby, 1833) in shrimp aquaculture effluents. Aquac. Res. 40, 1750–1758. https://doi.org/10.1111/j.1365-2109.2009.02280.x.

Petersen, J.K., Schou, O., Thor, P., 1995. Growth and energetics in the ascidian *Ciona intestinalis*. Mar. Ecol. Prog. Ser. 120, 175–184. https://doi.org/10.3354/meps120175.

Pimm, S.L., Lawton, J.H., Cohen, J.E., 1991. Food web patterns and their consequences. Nature 350, 669–674.

Piña-Ochoa, E., Høgslund, S., Geslin, E., Cedhagen, T., Revsbech, N.P., Nielsen, L.P., Schweizer, M., Jorissen, F., Rysgaard, S., Risgaard-Petersen, N., 2010. Widespread occurrence of nitrate storage and denitrification among Foraminifera and Gromiida. PNAS 107, 1148–1153.

Post, D.M., 2002. The long and short of food-chain length. Trends Ecol. Evol. 17, 269–277. https://doi.org/10.1016/S0169-5347(02)02455-2.

Pozzato, L., van Oevelen, D., Moodley, L., Soetaert, K., Middelburg, J.J., 2013. Sink or link? The bacterial role in benthic carbon cycling in the Arabian Sea's oxygen minimum zone. Biogeosciences 10, 6879–6891. https://doi.org/10.5194/bg-10-6879-2013.

Purinton, B.L., DeMaster, D.J., Thomas, C.J., Smith, C.R., 2008. ^{14}C as a tracer of labile organic matter in Antarctic benthic food webs. Deep-Sea Res. II 55, 2438–2450. https://doi.org/10.1016/J.DSR2.2008.06.004.

R-Core Team, 2017. R: A Language and Environment for Statistical Computing.

Raghukumar, C., Sheelu, G., Loka Bharathi, P., Nair, S., Mohandass, C., 2001. Microbial biomass and organic nutrients in the deep-sea sediments of the Central Indian Ocean Basin. Mar. Georesour. Geotechnol. 19, 1–16.

Ramirez-Llodra, E., Tyler, P.A., Baker, M.C., Bergstad, O.A., Clark, M.R., Escobar, E., Levin, L.A., Menot, L., Rowden, A., Smith, C.R., van Dover, C.L., 2011. Man and the last great wilderness: Human impact on the deep sea. PLoS One 6, e22588. https://doi.org/10.1371/journal.pone.0022588.

Randall, R., 2002. Using allometry with fish size to estimate production to biomass (P/B) ratios of salmonid poulations. Ecol. Freshw. Fish 11, 196–202.

Ren, J.S., Ross, A.H., Hayden, B.J., 2006. Comparison of assimilation efficiency on diets of nine phytoplankton species of the greenshell mussel *Perna canaliculus*. J. Shellfish Res. 25, 887–892.

Resgalla, C., Brasilde, E.S., Salomão, L.C., 2007. The effect of temperature and salinity on the physiological rates of the mussel *Perna perna* (Linnaeus 1758). Brazil. Arch. Biol. Technol. 50, 543–556. https://doi.org/10.1590/S1516-89132007000300019.

Rex, M.A., Etter, R.J., Morris, J.S., Crouse, J., McClain, C.R., Johnson, N.A., Stuart, C.T., Deming, J.W., Thies, R., Avery, R., 2006. Global bathymetric patterns of standing stock and body size in the deep-sea benthos. Mar. Ecol. Prog. Ser. 317, 1–8. https://doi.org/10.3354/meps317001.

Rice, A.L., Thurston, M.J.H., Bett, B.J., 1994. The IOSDL DEEPSEAS program: Introduction and photographic evidence for the presence and absence of a seasonal input of phytodetritus at contrasting abyssal sites in the northeastern Atlantic. Deep-Sea Res. 41, 1305–1320.

Roberts, D., Gebruk, A., Levin, V., Manship, B.A.D., 2000. Feeding and digestive strategies in deposit-feeding holothurians. Oceanogr. Mar. Biol. 38, 257–310.

Rodrigues, N., Sharma, R., Nagender Nath, B., 2001. Impact of benthic disturbance on megafauna in Central Indian Basin. Deep-Sea Res. II 48, 3411–3426. https://doi.org/10.1016/S0967-0645(01)00049-2.

Rowe, G.T., Deming, J.W., 1985. The role of bacteria in the turnover of organic carbon in deep- sea sediments. J. Mar. Res. 43, 925–950. https://doi.org/10.1357/002224085788453877.

Savari, A., Lockwood, A.P.M., Sheader, M., 1991. Variations in the physiological state of the common cockle (*Cerastoderma edule* (L.)) in the laboratory and in Southampton water. J. Molluscan Stud. 57, 33–44. https://doi.org/10.1093/mollus/57.1.33.

Schriever, G., 1990. Cruise Report DISCOL 2, Sonne-Cruise 64. Callao/Peru - Valparaiso/Chile 02.09. - 02.10.1989. Hamburg.

Schriever, G., Koschinsky, A., Bluhm, H., 1996. Cruise Report ATESEPP. Impacts of potential technical interventions on the deep-sea ecosystem of the southeast Pacific off Peru. Sonne Cruise 106. January 1 – March 9, 1996. Balboa/Panama - Balboa/Panama. Hamburg.

Schriever, G., Thiel, H., 1992. Cruise report DISCOL 3, Sonne-Cruise 77. Balboa/Panama - Balboa/Panama 26.01. - 27.02.1992. Hamburg.

Sejr, M.K., Petersen, J.K., Jensen, K.T., Rysgaard, S., 2004. Effects of food concentration on clearance rate and energy budget of the Arctic bivalve *Hiatella arctica* (L) at subzero temperature. J. Exp. Mar. Bio. Ecol. 311, 171–183. https://doi.org/10.1016/j.jembe.2004.05.005.

Sharma, R., Nagender Nath, B., Parthiban, G., Jai Sankar, S., 2001. Sediment redistribution during simulated benthic disturbance and its implications on deep seabed mining. Deep-Sea Res. II 48, 3363–3380. https://doi.org/10.1016/S0967-0645(01)00046-7.

Shirayama, Y., 1992. Respiration rates of bathyal meiobenthos collected using a deep-sea submersible SHINKA12000. Deep-Sea Res. 39, 781–788.

Shulse, C.N., Maillot, B., Smith, C.R., Church, M.J., 2017. Polymetallic nodules, sediments, and deep waters in the equatorial North Pacific exhibit highly diverse and distinct bacterial, archaeal, and microeukaryotic communities. Microbiologyopen 6, e00428. https://doi.org/10.1002/mbo3.428.

Simon-Lledó, E., Bett, B.J., Huvenne, V.A.I., Schoening, T., Benoist, N.M.A., Jones, D.O.B., 2019a. Ecology of a polymetallic nodule occurrence gradient: Implications for deep-sea mining. Limnol. Oceanogr. 64, 1883–1894. https://doi.org/10.1002/lno.11157.

Simon-Lledó, E., Bett, B.J., Huvenne, V.A.I., Köser, K., Schoening, T., Greinert, J., Jones, D.O.B., 2019b. Biological effects 26 years after simulated deep-sea mining. Sci. Rep. 9, 8040. https://doi.org/10.1038/s41598-019-44492-w.

Smaal, A.C.C., Vonck, A., 1997. Seasonal variation in C, N and P budgets and tissue composition of the mussel *Mytilus edulis*. Mar. Ecol. Prog. Ser. 153, 167–179. https://doi.org/10.3354/meps153167.

Smith-Ramesh, L.M., Moore, A.C., Schmitz, O.J., 2017. Global synthesis suggests that food web connectance correlates to invasion resistance. Glob. Chang. Biol. 23, 465–473. https://doi.org/10.1111/gcb.13460.

Smith, A.B., Stockley, B., 2005. The geological history of deep-sea colonization by echinoids: roles of surface productivity and deep-water ventilation. Proc. R. Soc. - Biol. Sci. 272, 865–869.

Smith, C.R., Berelson, W., Demaster, D.J., Dobbs, F.C., Hammond, D., Hoover, D.J., Pope, R.H., Stephens, M., 1997. Latitudinal variations in benthic processes in the abyssal equatorial Pacific: Control by biogenic particle flux. Deep-Sea Res. II 44, 2295–2317. https://doi.org/10.1016/S0967-0645(97)00022-2.

Smith, C.R., Glover, A.G., Treude, T., Higgs, N.D., Amon, D.J., 2015. Whale-fall ecosystems: Recent insights into ecology, paleoecology, and evolution. Ann. Rev. Mar. Sci. 7, 571–596. https://doi.org/10.1146/annurev-marine-010213-135144.

Smith, C.R., Hoover, D.J., Doan, S.E., Pope, R.H., Demaster, D.J., Dobbs, F.C., Altabet, M. A., 1996. Phytodetritus at the abyssal sea floor across 10° of latitude in the central equatorial Pacific. Deep-Sea Res. II 43, 1309–1338. https://doi.org/10.1016/0967-0645(96)00015-X.

Smith, K.L., 1978. Metabolism of the abyssopelagic rattail *Coryphaenoides armatus* measured in situ. Nature 274, 362–364. https://doi.org/10.1038/274362a0.

Smith, K.L., Brown, N.O., 1983. Oxygen consumption of pelagic juveniles and demersal adults of the deep-sea fish *Sebastolobus altivelis*, measured at depth. Mar. Biol. 76, 325–332. https://doi.org/10.1007/BF00393036.

Smith, K.L., Druffel, E.R.M., 1998. Long time-series monitoring of an abyssal site in the NE Pacific: An introduction. Deep-Sea Res. II 45, 573–586. https://doi.org/10.1016/S0967-0645(97)00094-5.

Smith, K.L., Hessler, R.R., 1974. Respiration of benthopelagic fishes: In situ measurements at 1230 meters. Science 184, 72–73.

Smith, K.L., Laver, M.B., 1981. Respiration of the bathypelagic fish Cyclothone acclinidens. Mar. Biol. 61, 261–266. https://doi.org/10.1007/BF00401564.

Snider, L.J., Burnett, B.R., Hessler, R.R., 1984. The composition and distribution of meiofauna and nanobiota in a central North Pacific deep-sea area. Deep-Sea Res. A 31, 1225–1249.

Soliman, Y.S.S., Rowe, G.T., 2008. Secondary production of *Ampelisca mississippiana* Soliman and Wicksten 2007 (Amphipoda, Crustacea) in the head of the Mississippi Canyon, northern Gulf of Mexico. Deep-Sea Res. II 55, 2692–2698. https://doi.org/10.1016/j.dsr2.2008.07.019.

Sommer, S., Linke, P., Pfannkuche, O., Niemann, H., Treude, T., 2010. Benthic respiration in a seep habitat dominated by dense beds of ampharetid polychaetes at the Hikurangi Margin (New Zealand). Mar. Geol. 272, 223–232. https://doi.org/10.1016/j.margeo.2009.06.003.

Ståhl, H., Tenberg, A., Brunnegård, J., Hall, P.O., 2004. Recycling and burial of organic carbon in sediments of the Porcupine Abyssal Plain, NE Atlantic. Deep-Sea Res. I 51, 777–791. https://doi.org/10.1016/j.dsr.2004.02.007.

Stratmann, T., Lins, L., Purser, A., Marcon, Y., Rodrigues, C.F., Ravara, A., Cunha, M.R., Simon-Lledó, E., Jones, D.O.B., Sweetman, A.K., Köser, K., van Oevelen, D., 2018a. Abyssal plain faunal carbon flows remain depressed 26 years after a simulated deep-sea mining disturbance. Biogeosciences 15, 4131–4145. https://doi.org/10.5194/bg-15-4131-2018.

Stratmann, T., Mevenkamp, L., Sweetman, A.K., Vanreusel, A., van Oevelen, D., 2018b. Has phytodetritus processing by an abyssal soft-sediment community recovered 26 years after an experimental disturbance? Front. Mar. Sci. 59. https://doi.org/10.3389/fmars.2018.00059.

Stratmann, T., Voorsmit, I., Gebruk, A.V., Brown, A., Purser, A., Marcon, Y., Sweetman, A.K., Jones, D.O.B., van Oevelen, D., 2018c. Recovery of Holothuroidea population density, community composition and respiration activity after a deep-sea disturbance experiment. Limnol. Ocean. 63, 2140–2153. https://doi.org/10.1002/lno.10929.

Sulak, K.J., Wenner, C.A., Sedberry, G.R., Van Guelpen, L., 1985. The life history and systematics of deep-sea lizard fishes, genus Bathysaurus (Synodontidae). Can. J. Zool. 63, 623–642.

Sweetman, A.K., Smith, C.R., Shulse, C.N., Maillot, B., Lindh, M., Church, M.J., Meyer, K. S., Oevelen, D., Stratmann, T., Gooday, A.J., van Oevelen, D., Stratmann, T., Gooday, A.J., 2019. Key role of bacteria in the short-term cycling of carbon at the abyssal seafloor in a low particulate organic carbon flux region of the eastern Pacific Ocean. Limnol. Oceanogr. 64, 694–713. https://doi.org/10.1002/lno.11069.

Sweetman, A.K., Thurber, A.R., Smith, C.R., Levin, L.A., Mora, C., Wei, C.-L., Gooday, A. J., Jones, D.O.B., Rex, M., Yasuhara, M., Ingels, J., Ruhl, H.A., Frieder, C.A., Danovaro, R., Würzberg, L., Baco, A., Grupe, B.M., Pasulka, A., Meyer, K.S., Dunlop, K.M., Henry, L.-A., Roberts, J.M., 2017. Major impacts of climate change on deep-sea benthic ecosystems. Elem. Sci. Anth. 5, 4. https://doi.org/10.1525/elementa.203.

Tatián, M., Sahade, R., Mercuri, G., Fuentes, V.L., Antacli, J.C., Stellfeldt, A., Esnal, G.B., 2008. Feeding ecology of benthic filter-feeders at Potter Cove, an Antarctic coastal ecosystem. Polar Biol. 31, 509–517. https://doi.org/10.1007/s00300-007-0379-7.

Thiel, H., Schriever, G., Borowski, C., Bussau, C., Hansen, D., Melles, J., Post, J., Steinkamp, K., Watson, K., 1989. Cruise-Report DISCOL 1, SONNE - Cruise 61. Hamburg.

Tilot, V., 1992. La structure des assemblages mégabenthiques d'une province à nodules polymétalliques de l'océan Pacifique tropical est. PhD-Thesis. Université de Bretagne Occidentale.

Thurber, A.R., Levin, L.A., Orphan, V.J., Marlow, J.J., 2012. Archaea in metazoan diets: Implications for food webs and biogeochemical cycling. ISME Journal 6, 1602–1612. https://doi.org/10.1038/ismej.2012.16.

Treude, T., Janssen, F., Queisser, W., Witte, U., 2002. Metabolism and decompression tolerance of scavenging lysianassoid deep-sea amphipods. Deep-Sea Res. I 49, 1281–1289. https://doi.org/10.1016/S0967-0637(02)00023-7.

Tully, B.J., Heidelberg, J.F., 2013. Microbial communities associated with ferromanganese nodules and the surrounding sediments. Front. Microbiol. 4, 1–10. https://doi.org/10.3389/fmicb.2013.00161.

van Oevelen, D., Duineveld, G.C.A., Lavaleye, M., Mienis, F., Soetaert, K., Heip, C.H.R., 2009. The cold-water coral community as hotspot of carbon cycling on continental margins: A food-web analysis from Rockall Bank (northeast Atlantic). Limnol. Oceanogr. 54, 1829–1844. https://doi.org/10.4319/lo.2009.54.6.1829.

van Oevelen, D., Bergmann, M., Soetaert, K., Bauerfeind, E., Hasemann, C., Klages, M., Schewe, I., Soltwedel, T., Budaeva, N.E., 2011a. Carbon flows in the benthic food web at the deep-sea observatory HAUSGARTEN (Fram Strait). Deep-Sea Res. I 58, 1069–1083. https://doi.org/10.1016/j.dsr.2011.08.002.

van Oevelen, D., Soetaert, K., Garcia, R., de Stigter, H.C., Cunha, M.R., Pusceddu, A., Danovaro, R., 2011b. Canyon conditions impact carbon flows in food webs of three sections of the Nazaré canyon. Deep-Sea Res. II 58, 2461–2476. https://doi.org/10.1016/j.dsr2.2011.04.009.

van Oevelen, D., Soetaert, K., Heip, C., 2012. Carbon flows in the benthic food web of the Porcupine Abyssal Plain: The (un)importance of labile detritus in supporting microbial and faunal carbon demands. Limnol. Oceanogr. 57, 645–664. https://doi.org/10.4319/lo.2012.57.2.0645.

van Oevelen, D., Soetaert, K., Middelburg, J.J., Herman, P.M.J., Moodley, L., Hamels, I., Moens, T., Heip, C.H.R., 2006. Carbon flows through a benthic food web: Integrating

biomass, isotope and tracer data. J. Mar. Res. 64, 453–482. https://doi.org/10.1357/002224006778189581.
van Oevelen, D., van den Meersche, K., Meysman, F.J.R., Soetaert, K., Middelburg, J.J., Vézina, A.F., 2010. Quantifying food web flows using linear inverse models. Ecosystems 13, 32–45. https://doi.org/10.1007/s10021-009-9297-6.
Vannier, J., Abe, K., Ikuta, K., 1998. Feeding in myodocopid ostracods: Functional morphology and laboratory observations from videos. Mar. Biol. 132, 391–408. https://doi.org/10.1007/s002270050406.
Vanreusel, A., Hilário, A., Ribeiro, P.A., Menot, L., Martínez Arbizu, P., et al., 2016. Threatened by mining, polymetallic nodules are required to preserve abyssal epifauna. Sci. Rep. 6, 26808. https://doi.org/10.1038/srep26808.
Velasco, L.A., Navarro, J.M., 2003. Energetic balance of infaunal (*Mulinia edulis* King, 1831) and epifaunal (*Mytilus chilensis* Hupé, 1854) bivalves in response to wide variations in concentration and quality of seston. J. Exp. Mar. Bio. Ecol. 296, 79–92. https://doi.org/10.1016/S0022-0981(03)00316-2.
Vézina, A.F., Platt, T., 1988. Food web dynamics in the ocean. I. Best-estimates of flow networks using inverse methods. Mar. Ecol. Prog. Ser. 42, 269–287.
Volz, J.B., Haffert, L., Haeckel, M., Koschinsky, A., Kasten, S., 2020. Impact of small-scale disturbances on geochemical conditions, biogeochemical processes and element fluxes in surface sediments of the eastern Clarion-Clipperton Zone, Pacific Ocean. Biogeosciences 17, 1113–1131. https://doi.org/10.5194/bg-17-1113-2020.
Vonnahme, T.R., Molari, M., Janssen, F., Wenzhöfer, F., Haeckel, M., Titschack, T., Boetius, A., 2020. Effects of a deep-sea mining experiment on seafloor microbial communities and functions after 26 years. Sci. Adv. 6, eaaz5922. https://doi.org/10.1126/sciadv.aaz5922.
Vranken, G., Heip, C.H.R., 1986. The productivity of marine nematodes. Ophelia 26, 429–442. https://doi.org/10.1080/00785326.1986.10422004.
Wiedicke, M.H., Weber, M.E., 1996. Small-scale variability of seafloor features in the northern Peru Basin: Results from acoustic survey methods. Mar. Geophys. Res. 18, 507–526.
Wigham, B.D., Galley, E.A., Smith, C.R., Tyler, P.A., 2008. Inter-annual variability and potential for selectivity in the diets of deep-water Antarctic echinoderms. Deep-Sea Res. II 55, 2478–2490.
Wigham, B.D., Hudson, I.R., Billett, D.S.M., Wolff, G.A., 2003. Is long-term change in the abyssal Northeast Atlantic driven by qualitative changes in export flux? Evidence from selective feeding in deep-sea holothurians. Prog. Oceanogr. 59, 409–441. https://doi.org/10.1016/j.pocean.2003.11.003.
Witte, U., Graf, G., 1996. Metabolism of deep-sea sponges in the Greenland-Norwegian Sea. J. Exp. Mar. Bio. Ecol. 198, 223–235. https://doi.org/10.1016/0022-0981(96)00006-8.
WoRMS Editorial Board, 2019. World Register of Marine Species. [WWW Document]. VLIZ. 10.14284/170.
Woulds, C., Bell, J.B., Glover, A.G., Bouillon, S., Brown, L.S., 2020. Benthic carbon fixation and cycling in diffuse hydrothermal and background sediments in the Bransfield Strait, Antarctica. Biogeosciences 17, 1–12. https://doi.org/10.5194/bg-17-1-2020.
Wright, J.R., Hartnoll, R.G., 1981. An energy budget for a population of the limpet *Patella vulgata*. J. Mar. Biol. Assoc. UK 61, 627–646. https://doi.org/10.1017/S0025315400048098.
Yu, Z., Hu, C., Zhou, Y., Li, H., Peng, P., 2013. Survival and growth of the sea cucumber *Holothuria leucospilota* Brandt: A comparison between suspended and bottom cultures in a subtropical fish farm during summer. Aquac. Res. 44, 114–124. https://doi.org/10.1111/j.1365-2109.2011.03016.x.
Zeng, Q., Huang, D., Lin, R., Wang, J., 2018. Deep-sea metazoan meiofauna from a polymetallic nodule area in the Central Indian Ocean Basin. Mar. Biodivers. 48, 395–405. https://doi.org/10.1007/s12526-017-0778-0.
Zhou, Y., Yang, H., Liu, S., Yuan, X., Mao, Y., Liu, Y., Xu, X., Zhang, F., 2006. Feeding and growth on bivalve biodeposits by the deposit feeder *Stichopus japonicus* Selenka (Echinodermata: Holothuroidea) co-cultured in lantern nets. Aquaculture 256, 510–520. https://doi.org/10.1016/j.aquaculture.2006.02.005.